2418 J. Med. Chem. 2010, 53, 2418–2432
DOI: 10.1021/jm901441b

Journal of Medicinal Chemistry Article

Novel Diamidino-Substituted Derivatives of Phenyl Benzothiazolyl and Dibenzothiazolyl Furans and Thiophenes: Synthesis, Antiproliferative and DNA Binding Properties

Livio Racané,[‡] Vesna Tralić-Kulenović,[‡] Sandra Kraljević Pavelić,[§] Ivana Ratkaj,[§] Paul Peixoto,[¶] Raja Nhili,[¶] Sabine Depauw,[¶] Marie-Paule Hildebrand,[¶,⊥] Marie-Hélène David-Cordonnier,*[,¶] Krešimir Pavelić,[§] and Grace Karminski-Zamola*[,†]

[†]*Department of Organic Chemistry, Faculty of Chemical Engineering and Technology, University of Zagreb, Marulićev trg 20, P.O. Box 177, HR-10000 Zagreb, Croatia,* [‡]*Department of Applied Chemistry, Faculty of Textile Technology, University of Zagreb, baruna Filipovića 28a 10000 Zagreb, Croatia,* [§]*Department of Biotechnology, University of Rijeka, Trg braće Mažuranića 10, 51000 Rijeka, Croatia,* [¶]*INSERM U837, Jean-Pierre Aubert Research Centre (JPARC), Team "Molecular and Cellular Targeting for Cancer Treatment", IRCL, Place de Verdun, F-59045 Lille cedex, France, and* [⊥]*Institut pour la Recherche sur le Cancer de Lille (IRCL), Place de Verdun, F-59045 Lille cedex, France*

Received September 29, 2009

A series of new diamidino-, diisopropylamidino-, and diimidazolinyl-substituted derivatives of phenyl benzothiazolyl and dibenzothiazolyl furans and thiophenes were successfully prepared and evaluated for their antiproliferative activity on tumor cell lines in vitro, DNA binding propensity, and sequence selectivity as well as cellular distribution. A strong antiproliferative effect of the tested compounds was observed on all tested cell lines in a concentration-dependent response pattern. In general, imidazolinyl-substituted derivatives and/or the thiophene core were in correlation with increased antiproliferative activity. Two compounds (**2b** and **3b**) were chosen for biological studies due to their differential antiproliferative properties. The DNA binding properties of this new series of compounds were assessed and evidenced their efficient minor groove binding properties with preferential interaction at AT-rich sites. Both compounds also present nuclear subcellular localization, suggesting that their cellular mode of action implies localization in the DNA compartment and direct inhibition of DNA replication and induction of apoptosis.

Introduction

In the last two decades, several heterocyclic compounds from the series of benzothiazoles were synthesized and their biological and pharmacological activity has consequently been investigated. These compounds were extensively studied for their antiallergic,[1] anti-inflammatory,[1,2] antitumor,[3−7] and analgesic[8,9] activities. Considering their mechanism of action, it was shown that benzothiazole derivatives act as tyrosine kinase[10−13] and topoisomerases I and II inhibitors.[14,15] Therefore, various benzothiazole compounds are considerably interesting due to their diverse pharmaceutical uses. A novel series of optically active thiourea and their 2-aminobenzothiazole derivatives were recently reported to exert a strong in vitro cytotoxicity against mouse Ehrlich Ascites carcinoma (EAC) and two human cancer cell lines MCF-7[a] and HeLa. In the alkaline comet assay, some of these compounds showed dose-dependent DNA damaging activity.[16] Further, the newly prepared 2-acetyl-3-(6-methoxybenzothiazo)-2-yl-aminoacrylonitrile showed significant antiproliferative activity and strongly induced programmed cell death in leukemia cells.[17] The most recent article on the synthesis of corresponding amino phenyl-substituted benzothiazoles described the identification of promising scaffolds that are able to inhibit different kinases with IC_{50} values in the nanomolar range.[18] Besides the benzothiazole core and its numerous potential biological implications, the central rings and attached substituents play a major role in the binding affinity and selectivity. Indeed, for the particular case of DNA binding of benzothiazole derivatives, engrafting amidine extremities to those structures, as positively charged substituents, orients the function of the molecule toward the binding to an electronegatively charged biological molecule such as DNA in a manner similar to that of berenil, pentamidine, stilbamidine, furamidine, and other diamidine heterocycles.[19,20] Such diamidine, or other imidazoline, charge effect was particularly well-studied for the furamidine aromatic diamidine series developed by Boykin's lab. Particularly, the presence of terminal charges was shown to facilitate the binding of the molecule to the minor groove of the DNA helix but also the cellular distribution of the compounds toward the nucleus.[21,22] Positively charged extremities are not the sole structural elements for strong DNA binding, and the three-dimensional organization of the molecule is crucial for sequence-selective DNA binding. It should ideally have a crescent shape,

*To whom correspondence should be addressed. Phone: +33 3 20 16 92 23. Fax: +33 3 20 16 92 29. E-mail: marie-helene.david@inserm.fr. Phone: ++38514597215. Fax: ++39514597224. E-mail: gzamola@fkit.hr.

[a]Abbreviations: bp, base pair; BPE, buffer phosphate EDTA; CD, circular dichroism; CT-DNA, calf thymus DNA; cpd, compound; dATP, deoxyadenosine triphosphate; dGTP, deoxyguanosine triphosphate; DMEM, Dulbecco's modified Eagle medium; DMSO, dimethyl sulfoxide; EDTA, ethylene diamine tetraacetic acid; FBS, fetal bovine serum; HeLa, cervical carcinoma; HEp-2, epidermoid carcinoma, larynx; HepG2, hepatocellular carcinoma; HP, hairpin; HT-29, human colon carcinoma cells; ICD, induced circular dichroism; JK, normal diploid human fibroblasts; MCF-7, breast epithelial adenocarcinoma, metastatic; MiaPaCa-2, pancreatic carcinoma; MTT, 3-(4,5-dimethylthiazole-2-yl)-2,5-diphenyl tetrazolium bromide, SW620, colorectal adenocarcinoma, metastatic; TBE, tris borate EDTA; T_m, melting temperature.

 Published on Web 02/19/2010

Scheme 1

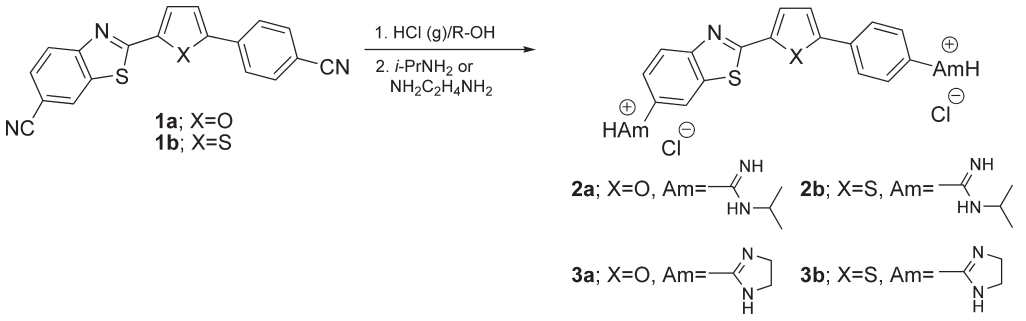

Scheme 2

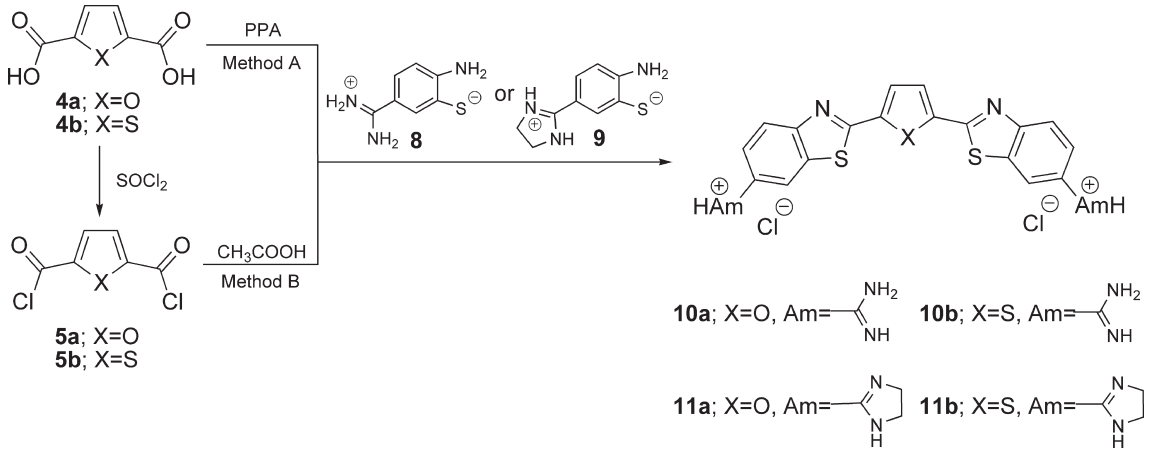

which allows the molecule to optimally fit the curve of the DNA minor groove to optimize both van der Waals and electrostatic contacts[23] even if some linear derivatives could also fit the minor groove through an original dimerization process, as evidenced for dication 4,4′-(pyrimidine-2,5-diyl)dibenzimidamide (DB1242),[23] or mediated through a water molecule as for the semilinear dicationic compounds 2-(4′-carbaminidoylbiphenyl-4-yl)-1*H*-benzo[*d*]imidazole-6-carboximidamide (DB921)[24] and 2-[4-(4-carbaminidoylphenoxy)phenyl]-1*H*-benzo[*d*]imidazole-6-carboximidamide (RT-29).[25]

Our previously obtained results showed that antiproliferative activity of cyano-, amidino-,[26] and amino[27]-substituted 2-phenylbenzothiazole derivatives strongly depends on the position of the substituent on the 2-phenylbenzothiazole skeleton, as well as on the type of amidino substituent attached. We found that, in a series of unsubstituted, *N*-isopropyl-substituted, as well as 2-imidazolinyl mono- and bisamidino derivatives of 2-phenylbenzothiazole, *N*-isopropyl-substituted amidine possesses less pronounced antiproliferative activity on tested tumor cells.

In relation with the above considerations, we designed and efficiently synthesized new diamidino-, diisopropylamidino-, and diimidazolinyl-substituted derivatives of phenyl benzothiazolyl and dibenzothiazolyl furans and thiophenes and evaluated their antiproliferative activity on tumor cell lines in vitro, DNA binding propensity, and sequence selectivity as well as cellular distribution. In addition, two compounds were chosen according to their differential effect for further biological studies, including the cell cycle analysis and apoptosis induction in order to reveal a more detailed picture on the possible antiproliferative mechanisms and/or targets.

Results and Discussion

Chemistry. The synthesis of the bisamidino-substituted benzothiazolyl derivatives was performed by two different approaches according to Schemes 1 and 2. Unsymmetrical bisamidino monobenzothiazolyl derivatives **2a**−**3b** were prepared from corresponding bisnitriles **1a** and **1b** by Pinner reaction previously described.[28] Following this approach for the synthesis of symmetrical bisamidino dibenzothiazolyl derivatives, the corresponding bisnitriles have to be prepared. By condensation reaction of 4-amino-3-sulfanylbenzonitrile[29] with dichloride of 2,5-furandicarboxylic acid, only bisnitrile **7** was prepared. Unfortunately, this approach failed when bisnitrile **7** was employed in the first step of the Pinner reaction due to its very low solubility even by using solvents such as 2-methoxyethanol and 2-(2-ethoxyethoxy)-ethanol and prolonged reaction time up to 3 weeks. The compound **7** did not convert into an imidoyl ether hydrochloride, and only a starting nitrile was recovered.

Recently, a second approach for the synthesis of amidino-substituted benzothiazolyl derivatives was developed.[30] We found a simple and efficient method for the synthesis of amidino **8** and 2-imidazolinyl-substituted 2-aminothiophenol **9** as the key precursor for this new synthetic approach outlined in Scheme 2. Condensation reaction of commercially available 2,5-furan and 2,5-thiophene dicarboxylic acid and amidino-substituted 2-aminothiophenole **8** was performed in polyphosphoric acid (Method A). The bisamidino dibenzothiazolyl compounds **10a**−**11b** were isolated as hydrochloride salts in a low to moderate yield of about 30−60%. To improve the yield, we tried to carry out the reaction of amidino-substituted 2-aminothiophenole **8** with

Table 1. Inhibition Effects of Compounds **2a**−**11b** on the Growth of Tumor Cells In Vitro[a]

	IC_{50}[b] (μM)						
	cell lines						
substance no.	HeLa	MCF-7	HEp-2	HepG2	SW620	MiaPaCa-2	JK
2a	13.91	0.24	51.39	72.43	50.56	0.50	61.05
2b	4.11	0.04	30.73	48.19	38.13	0.04	8.72
3a	0.13	0.03	0.37	0.40	0.39	< 0.01	0.02
3b	0.05	0.17	0.15	0.09	0.19	0.17	0.01
10a	6.52	0.19	> 100	7.97	> 100	0.01	0.09
10b	0.15	0.05	0.47	0.29	0.65	< 0.01	< 0.01
11a	4.89	0.37	> 100	30.53	> 100	0.06	0.07
11b	0.12	0.29	0.17	0.21	0.27	0.06	< 0.01

[a] The results are presented as IC_{50} values in μM. The cell growth rate was evaluated by performing the MTT assay: experimentally determined absorbance values were transformed into a cell percentage growth (PG) using the formulas proposed by National Cancer Institute and described previously in Gazivoda et al.[39] [b] IC_{50}; 50% inhibitory concentration, or compound concentration required to inhibit tumor cell proliferation by 50%. The IC_{50} values were calculated from dose−response curves using linear regression analysis by fitting the mean test concentrations that give PG values above and below the reference value. If, however, all of the tested concentrations produce PGs exceeding the respective reference level of effect (e.g., PG value of 50) for a given cell line, the highest tested concentration is assigned as the default value (> 100). Each test point was performed in quadruplicate in three individual experiments.

corresponding diacyl chlorides **5a** and **5b** in acetic acid (Method B). Conversion of furan and thiophene dicarboxylic acids into diacyl chlorides was achieved with thionyl chloride quantitatively, and the corresponding dichlorides were used in the condensation reaction. The overall yield for Method B was much better than in Method A, and for isolated diamidino dihydrochloride salts **10a**−**11b**, yield was 72−88%. The structures of the new compounds were confirmed by spectroscopic methods: IR, ^{1}H NMR, and ^{13}C NMR spectra, as well as MS and elemental analysis.

Antiproliferative Activity. The antiproliferative effect of compounds **2a**, **2b**, **3a**, **3b**, **10a**, **10b**, **11a**, and **11b** was evaluated in vitro on a panel of seven human cell lines derived from different cancer types including HeLa (cervical carcinoma), SW620 (colorectal adenocarcinoma, metastatic), MiaPaCa-2 (pancreatic carcinoma), MCF-7 (breast epithelial adenocarcinoma, metastatic), HEP-2 (epidermoid carcinoma, larynx), HepG2 (hepatocellular carcinoma), or JK (normal diploid human fibroblasts). Our previous results obtained by employing different benzothiazole derivatives have shown a strong antiproliferative activity for this class of compounds on several tumor cell lines.[7,26,27] The results obtained in this study were therefore partially expected and are summarized and presented in Table 1. The majority of compounds demonstrated a strong antiproliferative effect on all tested cell lines and exerted a concentration-dependent response pattern. Especially, this was observed on HeLa, MCF-7, and MiaPaCa-2 cell lines, where all compounds strongly inhibited the cell growth at submicromolar concentrations and higher (Table 1). In particular, the strongest antiproliferative effect was observed for three imidazolinyl-substituted derivatives **3a**, **3b**, and **11b** and for one isopropylamidino-substituted derivative with a thiophene core, **10b**. However, all of these compounds showed a nonselective cytotoxic activity. Interestingly, the isopropylamidino-substituted derivative **2a** was the least cytotoxic for normal human fibroblasts among the tested compound panel, while derivatives with a furan core, **10a** and **11a**, showed the weakest antiproliferative effect specifically on the growth of SW620 and HEp-2 cell lines. The isopropylamidino-substituted derivative **2b** with a thiophene core exerted a strong differential antiproliferative effect both on the MCF-7 and MiaPaCa-2 cells, while showing a lower cytotoxicity on normal human fibroblasts in comparison to other highly active compounds (Figure 2). All together, it has been concluded that

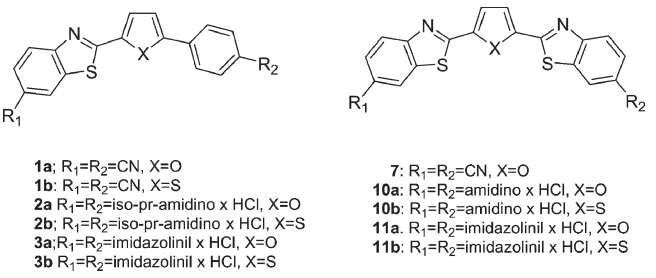

Figure 1. Cyano-disubstituted, isopropylamidino-disubstituted-, imdazolinyl-disubstituted 2-(4-phenyl)-5-(6-benzothiazolyl)furan and thiophene (**1a**−**3b**), cyano-disubstituted-, amidino-disubstituted, and imidazolinyl-disubstiuted 2,5-(6-benzothiazolyl)furans and thiophenes (**7**−**11b**).

imidazolinyl-substituted derivatives and/or the thiophene core are in correlation with increased antiproliferative activity of bisamidino-substituted benzothiazolyl derivatives. A similar observation was described by Racane et al., where the activity of imidazolinyl derivatives was better than that monitored for the isopropylamidino derivatives.[26] Further on, all tested compounds might act as DNA groove binders due to their angular structure (confirmed by further experiments and presented in the section DNA Binding Properties), making the cell DNA a dominant target for their antiproliferative activity. Additional mechanistic studies, including the cell cycle analysis and apoptosis induction assay, were thus performed in order to reveal a more detailed picture on the possible antiproliferative mechanisms and/or targets. Two derivatives were chosen for that purpose: (i) **2b** due to the observed differential effect on the growth of MCF-7 and MiaPaCa-2 cell lines and a lower cytotoxicity exerted on normal human fibroblasts in comparison to other tested compounds, and (ii) **3b**, as one imidazolinyl-substituted derivative with a thiophene core that showed less cytotoxic effect on MCF-7, MiaPaCa-2, and normal human fibroblasts.

Effects of 2b and 3b on the Cell Cycle of MiaPaCa-2 and MCF-7 Cell Lines. The results of the flow cytometric analysis revealed strong perturbations in the cell cycle of MiaPaCa-2 and MCF-7 induced upon treatments with different concentrations of **2b** and **3b** (Table 2). The observed perturbations varied for each substance and in dependence to the concentration used, substantiating the impact of structural differences and concentration on the activity.

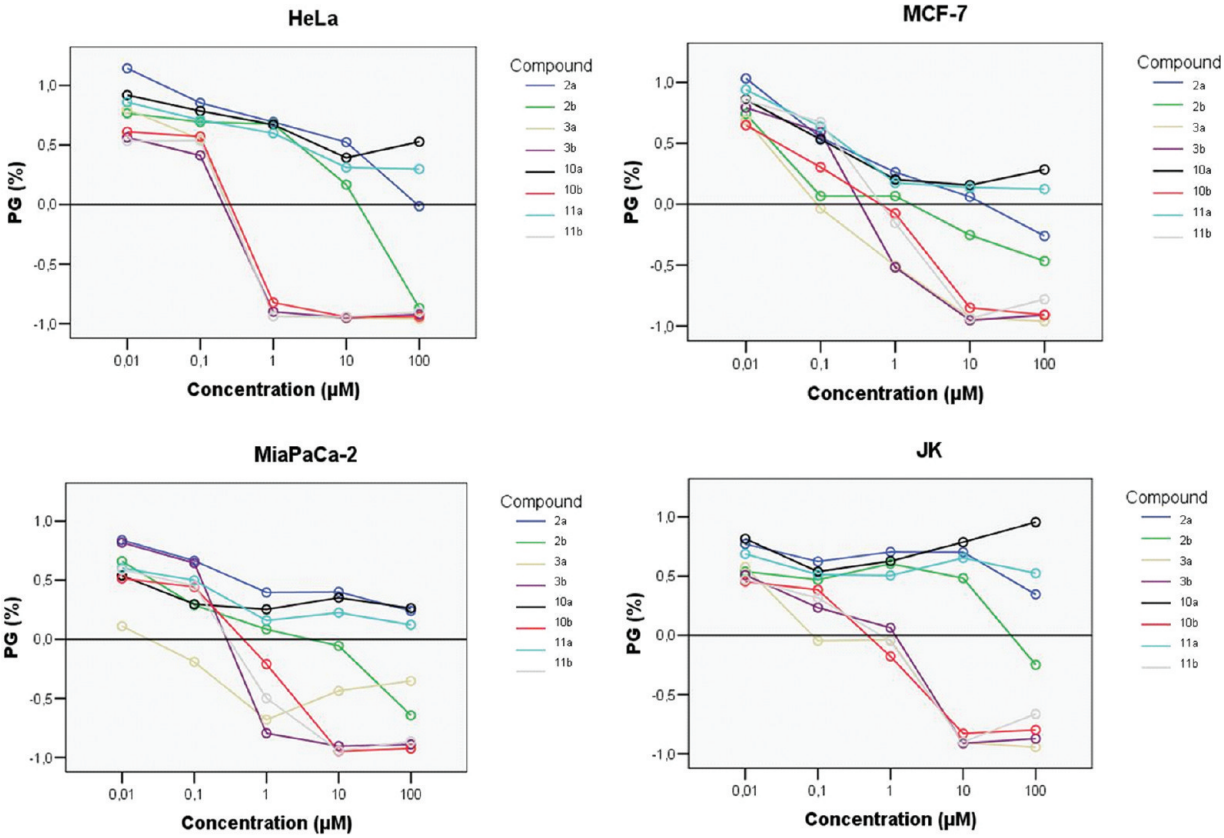

Figure 2. Concentration−response profiles obtained on HeLa, MCF-7, MiaPaCa-2, and JK cells treated with the tested compounds at different concentrations. The percentages of growth (PG) were calculated.

In MCF-7 cells (Table 2), the lower concentration of compound **2b** (10 μM) induced an increase in the S-phase population and a substantial decrease in the G2/M cell population accompanied by a moderate rise in the sub-G1 cell population. Oppositely, the higher tested concentration of compound **2b** (50 μM) induced a drastic accumulation of cells in the G2/M phase accompanied by a concomitant decrease of cells in the G1 phase and an accentuated increase of cell number in the sub-G1 phase. A same pattern was observed upon treatment of MCF-7 cells with compound **2b** at both tested concentrations after 48 h, which was accompanied by a drastic decrease of cell number in the S phase for treatment with higher **2b** concentration. It seems thus, that the main antiproliferative mechanism of **2b** depends on the concentration used and involves a cell cycle arrest in the S phase induced upon treatment with lower concentration and the G2/M delay upon treatment with higher concentration.

In MiaPaCa-2 cells (Table 2), compound **3b** (at concentration 1 μM) induced a marked increase in the G2/M phase after the 24 h treatment accompanied by a concomitant decrease in the G1 and S cell population. Similarly, an increase in the G2/M phase was induced after the 48 h treatment with the same concentration, even if an increase in the S phase was observed, as well. A marked increase in the sub-G1 was observed for both concentrations upon 24 and 48 h treatments. Additionally, MiaPaCa-2 cells treated with a higher concentration of **3b** (5 μM) after 48 h accumulated in the G1 phase, which was accompanied with a decrease in the G2/M population. The antiproliferative mechanism of **3b** on MiaPaCa-2 cells thus depends on the concentration used and involves a cell cycle arrest in the G2/M phase induced upon treatment with lower concentration, the G1 delay upon treatment with higher concentration, and a substantial rise of cells in the sub-G1 phase in all treatments.

In MCF-7 cells (Table 2), compound **3b** upon the 24 h treatment provoked a marked decrease in G1 population, which was more accentuated in the treatment with higher **3b** concentration. This G1 decrease was accompanied by a rise in sub-G1, S, and G2/M cell populations. Similarly, a decrease in the G1 population was observed for both tested concentrations upon the 48 h treatment, which was followed by a moderate rise of cells in the sub-G1 phase and a substantial rise of cells in the S phase. The antiproliferative mechanism of **3b** on MCF-7 cells is thus somewhat different in comparison to the activity observed on MiaPaCa-2 cells. It involves a moderate rise of cells in the sub-G1 phase in all treatments, a rise in cell number in the S-phase in all treatments, and a G2/M arrest upon the 48 h treatment with the higher concentration. Similar results were obtained with the class of cyano- and amidinobenzothiazole derivatives described in our previous paper, where both G1 and G2/M delays accompanied by a reduction of cell number in the S-phase were described.[31] However, the increase of cells in the S-phase observed in our experiments might be explained by previously described mechanisms of action for this class of compounds that include the hampering of DNA replication processes in the cytoplasm and nucleus (e.g., through inhibition of topoisomerase I and II and/or by direct binding to DNA).[20,31,32] Briefly, the damaged cells block the cell cycle prior to mitosis, and if the damage is too high, they ultimately die, which might be the case in our experiments, as well. Indeed, we observed that both compounds induced an

Table 2. Flow Cytometric Analysis of the MCF-7 and MiaPaCa-2 Cell Cycle upon the 24 and 48 h Treatments with Compound **2b** at Concentrations 10 and 50 μM and Compound **3b** at Concentrations of 1 and 5 μM[a]

compound **2b**				
cell line/treatment	cell percentage (% ± standard deviation)[c]			
MCF-7	sub-G1	G1	S	G2/M
control 24 h	2.4 ± 0.5	46.3 ± 2	31.8 ± 2.2	27.6 ± 0.9
10 μM 24 h	6.7 ± 0.1[b]	47.4 ± 1.4	41.5 ± 1.9[b]	9.5 ± 1[b]
50 μM 24 h	18.5 ± 5.3[b]	1.1 ± 0.7[b]	44.5 ± 6.4	63 ± 5.2[b]
control 48 h	2.7 ± 0.1	47 ± 2.4	41.4 ± 2.3	15.7 ± 0.8
10 μM 48 h	2.1 ± 0.1[b]	9.9 ± 4.6[b]	83.5 ± 2.1[b]	6.6 ± 2.4[b]
50 μM 48 h	8.6 ± 0.1[b]	54.5 ± 2.1	12.3 ± 0.5[b]	32.3 ± 1.3[b]
compound **3b**				
MiaPaCa-2				
control 24 h	15.2 ± 1.8	31.7 ± 1.6	50.1 ± 0.6	18.3 ± 1.1
1 μM 24 h	33.8 ± 1.4[b]	18.3 ± 0.6[b]	36.8 ± 2.5[b]	44.9 ± 2.1[b]
5 μM 24 h	21.8 ± 0.12[b]	37.9 ± 8.4	51.6 ± 2.3	10.5 ± 6.2
control 48 h	14.0 ± 0.5	44.6 ± 1.1	29.6 ± 1.5	27.4 ± 1.8
1 μM 48 h	55.1 ± 0.2[b]	11.4 ± 0.1[b]	44.7 ± 0.4[b]	43.9 ± 0.5[b]
5 μM 48 h	40.7 ± 0.5[b]	55.1 ± 2.1[b]	35 ± 1.4	10.4 ± 1.3[b]
MCF-7				
control 24 h	2.4 ± 0.5	44.8 ± 1.3	31.1 ± 2.8	23.9 ± 4.2
1 μM 24 h	10.1 ± 5.1	26.6 ± 1.5[b]	40.1 ± 1.6	34.2 ± 1.1
5 μM 24 h	8.6 ± 0.9[b]	8 ± 3.3[b]	45.8 ± 0.9[b]	46.2 ± 4.2[b]
control 48 h	2.6 ± 0.1	46.6 ± 1.8	38.8 ± 1.3	15.3 ± 1.3
1 μM 48 h	7.7 ± 0.1[b]	32.6 ± 1.2[b]	45.8 ± 1.3[b]	13.9 ± 1.3[b]
5 μM 48 h	6.3 ± 0.1[b]	9.9 ± 2.3[b]	69.7 ± 1.8[b]	20.5 ± 0.6[b]

[a] Cells were stained with propidium iodide and analyzed with Becton Dickinson FACScalibur flow cytometer (10 000 counts were measured for each condition). The results are presented as cell percentages (%). [b] Statistically significant: statistical analysis was performed in Microsoft Excel by using the ANOVA at $p < 0.05$. [c] The percentage of the cells in each cell cycle phase was based on the obtained DNA histograms and determined using the WinMDI 2.9 and Cylchred software.

increase of sub-G1 MCF-7 and MiaPaCa-2 cell populations, which is indicative of apoptosis. The most drastic rise in sub-G1 was, however, seen in MiaPaCa-2 cells treated with **3b**. The annexin V assay was hence performed to confirm apoptosis, and morphological changes of cells were monitored by microscopy.

Annexin V Assay. Due to high antiproliferative activity observed for tested compounds, the results of annexin V assay were expected and showed a marked increase in the number of apoptotic cells upon treatments with all tested concentrations of **2b** and **3b** (Table 3). However, higher concentrations were more effective in apoptosis induction in both cell lines upon the 48 h treatment. Therefore, the number of apoptotic MCF-7 and even more for MiaPaCa-2 cells, rose substantially upon the 24 h treatment with compound **3b**. A strong effect on apoptosis induction was observed for compound **2b** on the MCF-7 cells, as well, where the number of apoptotic cells reached 79% upon the 24 h treatment and 86% upon the 48 h treatment. Higher concentrations of compound **3b** induced a similar rise of apoptotic cells after 48 h in MCF-7 and MiaPaCa-2 cells, where it reached 74 and 81%, respectively.

The observed percentages are higher than percentages of cells in the sub-G1 phase documented in the cell cycle analysis probably because annexin V assay does not discriminate between diverse types of cell death mechanisms and it rather generally indicates dying cells. The cell death suppression is extremely relevant for tumor development and progression. The mechanisms of cell death and cell survival are complex and involve much more than apoptosis and/or necrosis with cross-talk and other programmed processes such as autophagy, postmitotic death, or entosis.[33,34] Indeed,

Table 3. Results of the Annexin V Assay Performed on MCF-7 and MiaPaCa-2 Cells upon 24 and 48 h Treatments with Compounds **2b** and **3b**[a]

compound **2b**		compound **3b**		
	MCF-7 (%)		MCF-7 (%)	MiaPaCa-2 (%)
control 24 h	15	control 24 h	9	18
10 μM	76	1 μM	40	57
50 μM	94	5 μM	54	68
control 48 h	13	control 48 h	8	15
10 μM	52	1 μM	26	42
50 μM	99	5 μM	82	96

[a] The results are presented as percentages of cells positive for annexin and/or propidium iodide (apoptotic cells) per total counted cell number.

99% of MCF-7 cells treated with higher concentration of **2b** were stained both green and red (Figure 3), which might be indicative for necrosis and apoptosis, while the cell cycle analysis for this treatment showed a rather moderate increase in the sub-G1 cell population. Moreover, MCF-7 cells treated with compound **2b** increased several times in volume (Figure 4), which is linked to the S and G2/M arrests revealed by the cell cycle analysis. Thus, MCF-7 cells probably died through a distinct cell death mechanism that involves the block of cells from S−G_2 transition upon treatment with lower **2b** concentration and impaired cell division through the G2/M phase arrest upon treatment with higher concentration of **2b**. It has already been shown that antitumor compounds might cause such a block of cells from the S−G_2 transition by decreasing the rate of DNA synthesis through diverse mechanisms, including inhibition of topoisomerase I[35] or DNA polymerase.[36] However, in this study,

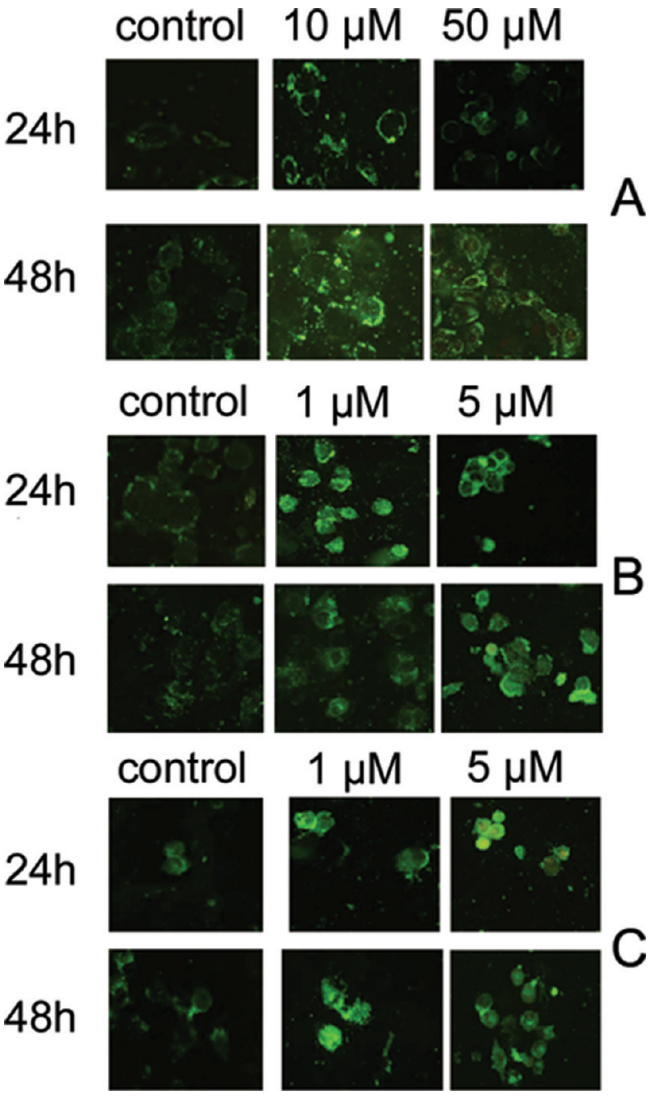

Figure 3. Representative fluorescence microscopy pictures of apoptotic MCF-7 (A,B) and MiaPaCa-2 (C) cells treated with compounds **2b** (A) and **3b** (B,C) after the 24 and 48 h treatments. The apoptotic cells are labeled with green fluorescein and/or red propidium iodide (control: untreated cells).

we have shown that neither one tested compound, including compounds **2b** and **3b**, exerted intercalative properties and/or topoisomerase I induced relaxation. Nevertheless, it has been shown that both compounds act as groove binders and thereby directly inhibit DNA replication and induce apoptosis (described later on in the text). Moreover, we showed that all compounds easily penetrate through the cell membrane and accumulate in the nucleus where they influence the DNA synthesis observed as sustained S or G2 arrest in the treatment of cells with **2b** and **3b**. The compound **3b**, however, accumulates as well in the perinucleus, probably causing additional perinuclear DNA destabilization (e.g., through interaction with other partners). This phenomenon might explain the observed difference in the mechanism of action that involves a stronger apoptotic response of cells treated with **3b** and accumulation in the sub-G1 phase. Indeed, a change of cell morphology that points to apoptosis (shrinkage of cells, chromatin condensation) was observed for both MCF-7 and MiaPaCa-2 cells treated with compound **3b** (Figures 3 and 4).

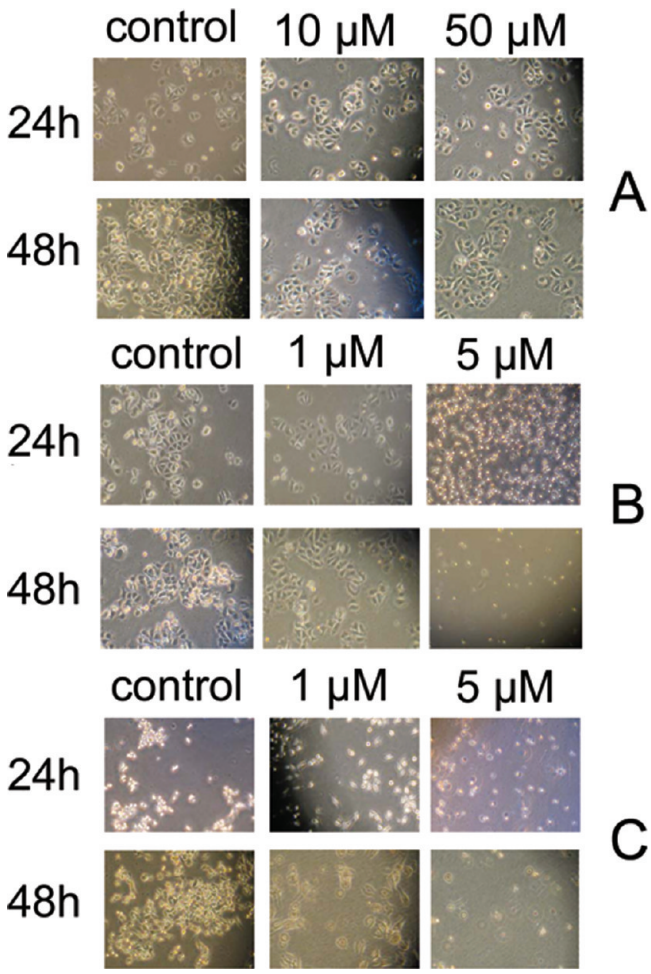

Figure 4. MCF-7 (A,B) and MiaPaCa-2 (C) cells treated with compounds **2b** (A) and **3b** (B,C) after 24 and 48 h treatments. MCF-7 cells treated with compound **2b** increased several times in volume, while a change of cell morphology that directly points to apoptosis (shrinkage of cells, chromatin condensation) was observed for MCF-7 and MiaPaCa-2 cells treated with compound **3b** (control: untreated cells).

Table 4. Variation of DNA Melting Temperature (ΔT_m) of CT-DNA or Poly(dAdT)$_2$ Induced by the Various Compounds (Cpd)

	ΔT_m[a] (°C)	
Cpd	CT-DNA	(dAdT)$_2$
2a	12.7	27.1
2b	14.2	26.5
3a	18.0	32.4
3b	13.9	24.3
10a	9.5	23.2
10b	7.6	5.1
11a	17.3	25.3
11b	2.3	1.4

[a] Variation of the T_m values for 20 μM of CT-DNA or poly(dAdT)$_2$ incubated with 2 μM of various compounds (drug/base pair ratio = 0.1) versus incubation alone. The reaction is conducted at room temperature in 1 mL of BPE buffer (6 mM Na_2HPO_4, 2 mM NaH_2PO_4, 1 mM EDTA, pH 7.1).

DNA Binding Properties. The DNA binding propensity for the new series of benzothiazole derivatives was first assessed using UV spectrometry. DNA melting temperature (Table 4) and modification of the absorption spectra of each compound in the presence or absence of CT-DNA (Supplementary Figure 1A) was first studied. A Benesi–Hildebrand derived plot of [CT-DNA]/($\varepsilon_{Free} - \varepsilon_{Obs}$) over

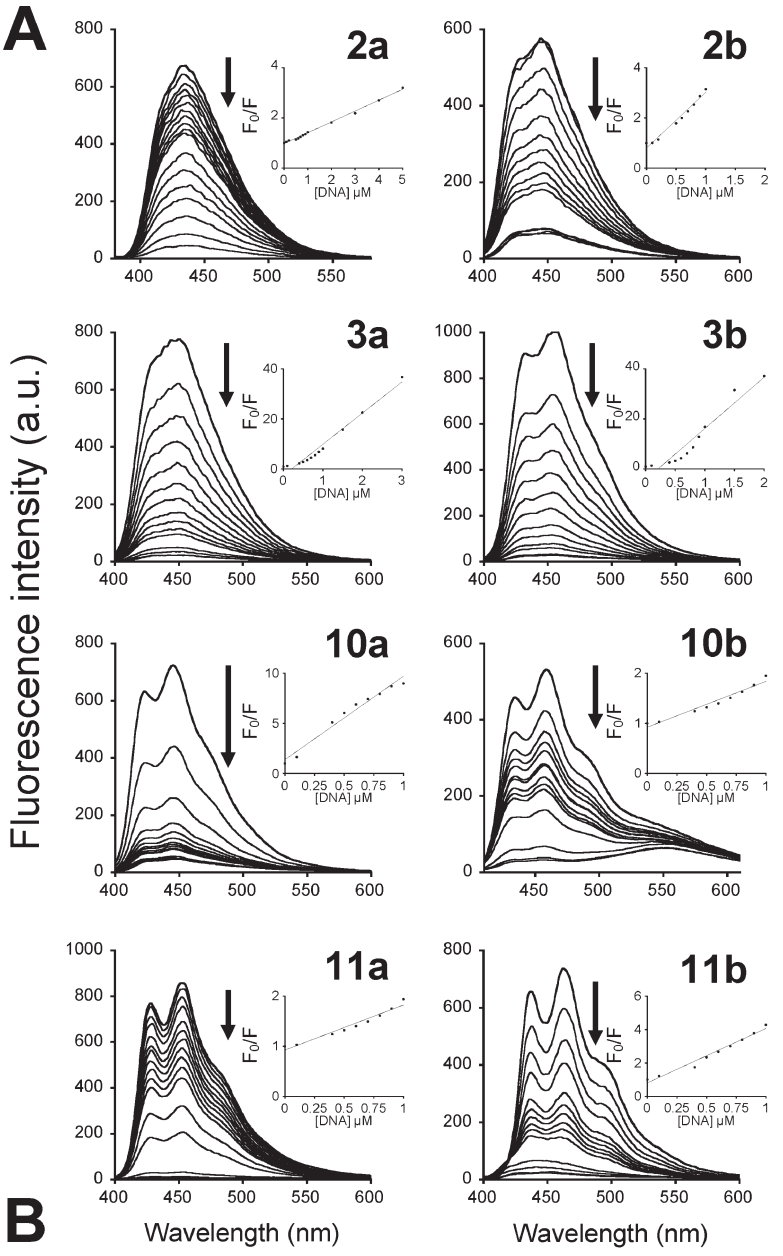

	Compounds							
	2a	**2b**	**3a**	**3b**	**10a**	**10b**	**11a**	**11b**
Ksv (M)	0.44	2.24	12.6	21.2	8.46	0.92	0.93	3.31
R²	0.996	0.978	0.970	0.923	0.974	0.959	0.959	0.976

Figure 5. Fluorescence quenching upon DNA binding. Panel A: Fluorescence measurements are expressed as arbitrary units (a.u.) over wavelength (nm). A fixed concentration of compounds (1 μM for **2b**, **3b**, and **10a** or 5 μM for the others) was incubated alone (upper lanes) or with increasing concentrations of CT-DNA from 1 to 30 μM (up to down arrows). The corresponding Stern−Volmer plots are presented as embedded panels expressing the decrease of fluorescence of the unbound compound (F_0/F) of CT-DNA concentration expressed in μM. Panel B: Stern−Volmer constants (K_{SV}). K_{SV} values for the various compounds are calculated from the slope and intercept values deduced from Stern−Volmer plots presented in panel A and are expressed in M.

[CT-DNA] was constructed where ε_{Free} and ε_{Obs} are the extinction coefficients for free compound and that obtained from UV−vis spectrometry measurement at the various CT-DNA concentrations ([CT-DNA]) (Supplementary Figure 1B). The ratio of intercept to slope gave the equilibrium constants for the formation of various drug/DNA complexes, which are presented in the bottom part of Supplementary Figure 1B). The binding constant evidenced that compounds **2a**, **2b**, **3a**, **3b**, and **11a** are the strongest DNA binders. The variation of melting temperature studies using CT-DNA identified compounds **2a**, **2b**, **3a**, **3b**, **10a**, and **11a** as strong DNA binders with ΔT_m of more than or

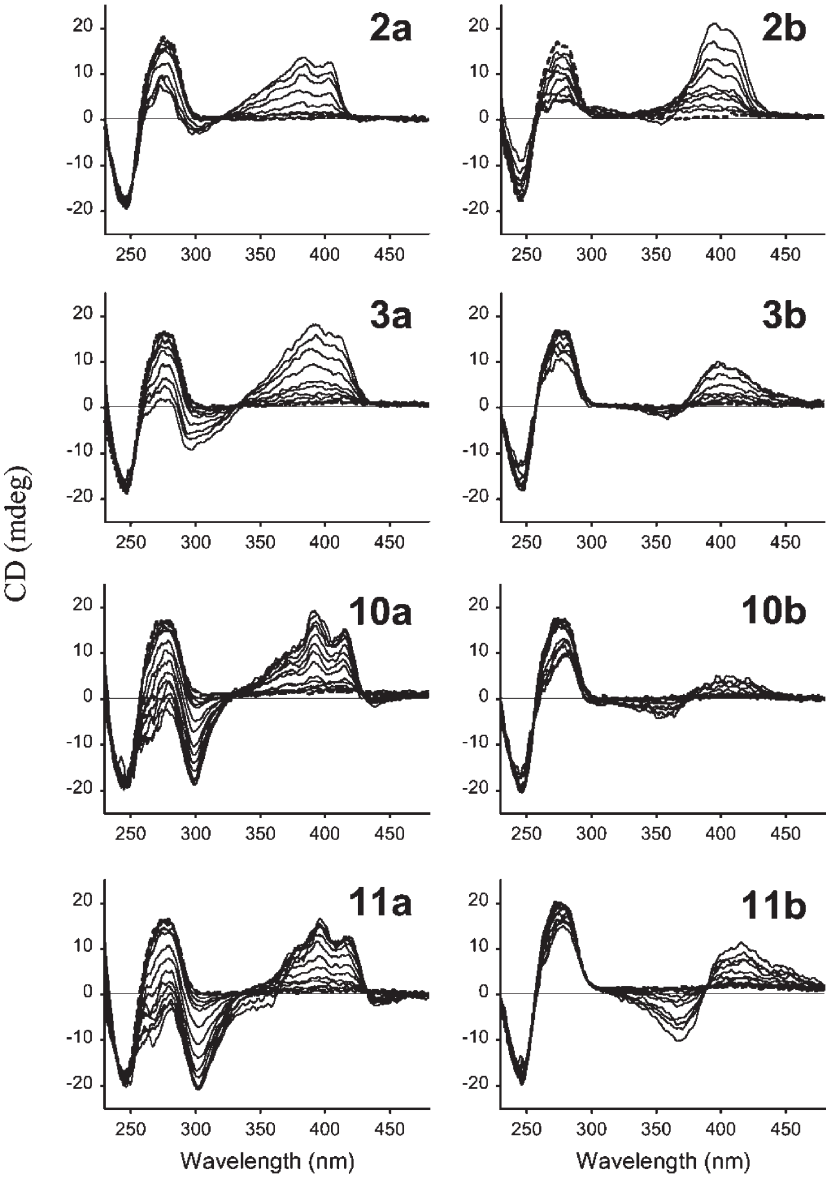

Figure 6. Circular dichroism measurements performed in the presence of CT-DNA. Graded concentrations of various benzothiazole derivatives from 1 to 25 μM (**2a** to **3b**) or from 1 to 50 μM (**10a** to **11b**) were added to samples containing CT-DNA alone (dashed bold lanes). Each lane corresponds to an average of three measurements.

around 10 °C at drug/CT-DNA ratios (r) of 0.1. The same studies performed using double-strand poly(dAdT)$_2$ (r = 0.1) evidenced the same series as very strong binders of AT-rich sequences.

All compounds present intrinsic fluorescence properties that could be used to evaluate their respective DNA binding propensities. Their DNA binding activity is associated with a decrease of the fluorescence intensities of benzothiazole derivatives with various intensities, as evidenced in Figure 5A. The quenching constants K_{SV} (Figure 5B) were deduced from Stern−Volmer plots (Figure 5A, embedded panels).

The binding mode (intercalation, groove binding) was then evaluated using circular dichroism (CD) measurements (Figure 6) and topoisomerase I induced relaxation assays (data not shown). The CD spectrum of CT-DNA (200 μM, dashed bold lane) presents the negative peak at ~245 nm and the positive peak at ~275 nm typical for a right-handed helix. This classical CT-DNA-induced CD spectrum dramatically changed upon addition of increasing concentration of compounds. Indeed, however, each compound failed to present any intrinsic CD (data not shown), a large positive induced CD (ICD) appears at around 400 nm, within the absorption band of the compound, as evidenced from Supplementary Figure 1. This positive ICD is very high, particularly for compounds **2a**, **2b**, **3a**, **3b**, **10a**, and **11a**, and may suggest a binding of the compound in one groove of the helix. This positive ICD is associated with a negative ICD at band around 300 nm for some compounds (**2a**, **3a**, **10a**, and **11a**), suggesting some differences in the DNA interaction between the furan (**a**) and the thiophene (**b**) series. Compounds **10b** and **11b** induce particular bisignate excitonic ICDs characterized by equal negative and positive values on either side of their respective absorption maxima. This only appears at the highest drug/DNA ratio and could possibly be due to exciton coupling interactions between closely bound chromophores as part of dye−dye interaction. We then focused on the ICD by increasing compounds **2a**, **2b**, **3a**, **3b**, **10a**, and **11a** on either poly(dAdT)$_2$ (Supplementary Figure 2A) or

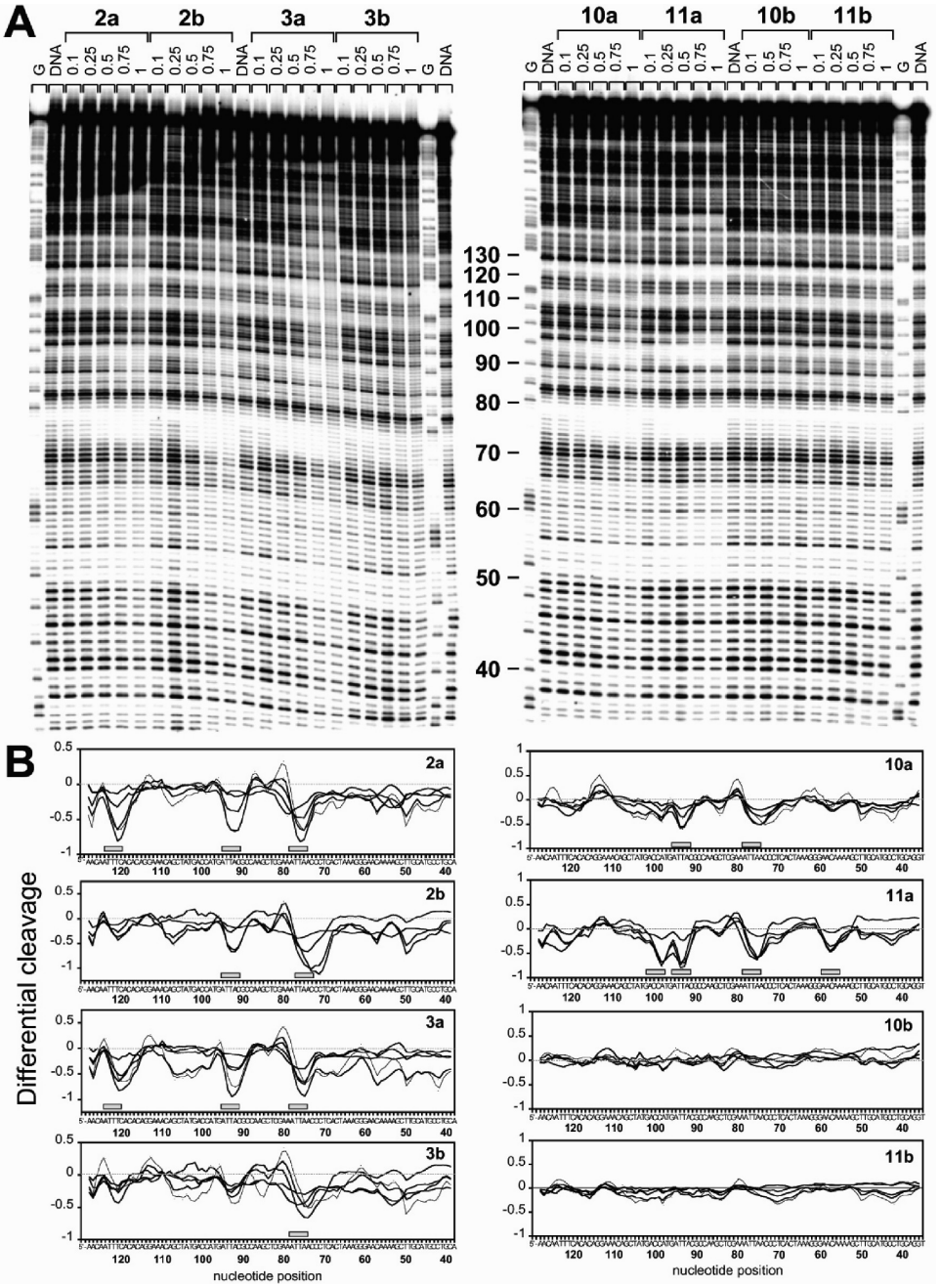

Figure 7. DNase I footprinting assays. Panel A: Radio-labeled 265 bp DNA fragment was incubated alone (lanes "DNA") or graded concentrations of the various indicated benzothiazole derivatives from 0.1 to 1 μM (as indicated on the top of each lanes). The G-track lanes labeled "G" were used as markers for guanines to locate the footprint areas and to establish the scale indicated from 40 to 130 bp. Panel B: Densitometric analysis. Differential cleavage plots derived from the gels are presented in (A). Gray boxes localize the sites protected on the gels.

poly(dGdC)$_2$ (Supplementary Figure 2B). Using poly-(dAdT)$_2$, the addition of increasing concentrations of each tested compound evidenced very strong positive ICD in the band of compound absorbance, as well as a strong drop on the positive CD from the DNA (270−280 nm). Such strong positive ICD in the absorption band of the compounds argues for a binding in one groove of the DNA helix. Using the highest concentrations of compounds (more than 20 μM and particularly with compounds **2b** and **3b**), a negative peak at ~365 nm appears that suggests a possible second mode of binding to the DNA (Figure 6). The possibility of a second binding mode was also suggested by the UV/visible absorption spectrometry experiments (Supplementary Figure 1) that showed an evolution of the CD spectra for drug concentrations > 20 μM with spectra losing the first isosbestic point obtained at lower drug concentrations (409 and 412 nm for **2b** and **3b**, respectively) for a second isosbestic point observed at higher wavelength using the highest drug/DNA ratios (418 and 432 nm for **2b** and **3b**, respectively). By contrast, oppositely signed CD bands in the visible spectral region using poly(dGdC)$_2$ may correspond to strong excitonic effects appearing only at the highest drug/DNA ratios using compounds **2a**, **2b**, and **3b** (more than 20 μM of CT-DNA). Altogether, the CD spectra give arguments for groove binding of compounds **2a**, **2b**, **3a**, **3b**, **10a**, and **11a** from CT-DNA experiments, more likely on AT-rich sequences.

Topoisomerase I induced relaxation assays were also performed as described in Peixoto et al.[37] to determine

possible DNA intercalation properties of the tested compounds. None of the compounds presented any typical DNA intercalation profile from this experiment (data not shown), comfirming the absence of intercalation between adjacent base pairs of CT-DNA shown CD experiments (Figure 6).

DNA Sequence Selectivity. Sequence-specific DNA binding properties were precisely assessed using DNase I footprinting assays (Figure 7 and Supplementary Figures 3−5). Revelation of the gels showed some protected regions (footprints) in the presence of increasing concentrations of compounds **2a**, **2b**, **3a**, **10a**, and **11a** and to a much lesser extent compound **3b** but no footprints in the presence of compounds **10b** and **11b** (Figure 7A). Densitometric analyses of the gels evidenced that the protected portions of the gel span AT-rich sequences (Figure 7B). Particularly, 5′-$_{78}$ATTA$_{75}$, 5′-$_{95}$ATTA$_{92}$, and 5′-$_{104}$ATTT$_{101}$ sites are well-recognized by the furan compounds **2a** and **3a**. Compound **11a** presents a more particular profile with recognition of sites 5′-$_{102}$ATTA$_{98}$ and 5′-$_{59}$AACA$_{56}$ additionally to the other 5′-$_{78}$ATTA$_{75}$ and 5′-$_{95}$ATTA$_{92}$ sites. The thiophene compounds present lesser (**2b** and **3b**) to no more (**10b**, **11b**) binding selectivity than their furan counterparts. Similarly, DNase I footprinting experiments performed using the 257 bp (Supplementary Figures 3 and 4) and 117 bp (Supplementary Figure 5) DNA fragments confirm the preference for AT-rich site recognition with some sequence selectivity depending on the A or T successions (Supplementary Figure 5) but also evidenced binding for compounds **2b** and **3a** on the 5′- AACT site, alighting the complexity of sequence selectivity of those compounds (Supplementary Figures 3 and 4).

Table 5. Variation of DNA Melting Temperature (ΔT_m) of Hairpin (HP) Oligonucleotides Induced by Various Compounds (Cpd)[a]

	ΔTm[b] (°C)				
Cpd	HP-ATTA	HP-AATT	HP-TTAA	HP-ACCA	HP-GCGC
2a	4.1	11.4	7.7	2.8	9.8
2b	5.7	10.1	6.7	2.6	4.1
3a	6.8	15.5	8.6	3.6	6.6
3b	0.8	3.5	2.1	1.5	3.5
10a	1.1	2.6	1.8	1.1	4.2
10b	3.3	1.8	0.6	0	0.6
11a	4.4	9.3	4.3	2.1	1.6
11b	1.1	0.4	0	0	0

[a] Different HP oligonucleotides containing in the stem the binding sites as specified. [b] Variation of the T_m values for 2 μM of 22-mer hairpin oligonucleotides forming a 9 bp stem that varies for the indicated 4-mer sequence incubated with 2 μM of the various compounds (drug/oligonucleotide ratio = 1) versus incubation alone. The reaction is conducted at room temperature in 1 mL of BPE buffer (6 mM Na_2HPO_4, 2 mM NaH_2PO_4, 1 mM EDTA, pH 7.1).

Binding to those DNA sequences was analyzed using melting temperature studies by employing hairpin (HP) oligonucleotides containing each of the sequences as single binding sites. Table 5 shows compounds **2a**, **2b**, **3a**, and **11a** as strong binders for AT-rich sequences: 5′-AATT, 5′-TTAA, and 5′ATTA sites, with a preference for 5′-AATT. However, some binding to GC-rich sites could also occur as evidenced using the HP-GCGC sequence using compounds **2a** to **10a**. Mixed 5′-ACCA sequences were also tested but showed weaker DNA stabilization potencies using the tested compounds.

Cellular Penetration and Distribution. In order to determine whether different compounds might efficiently pass

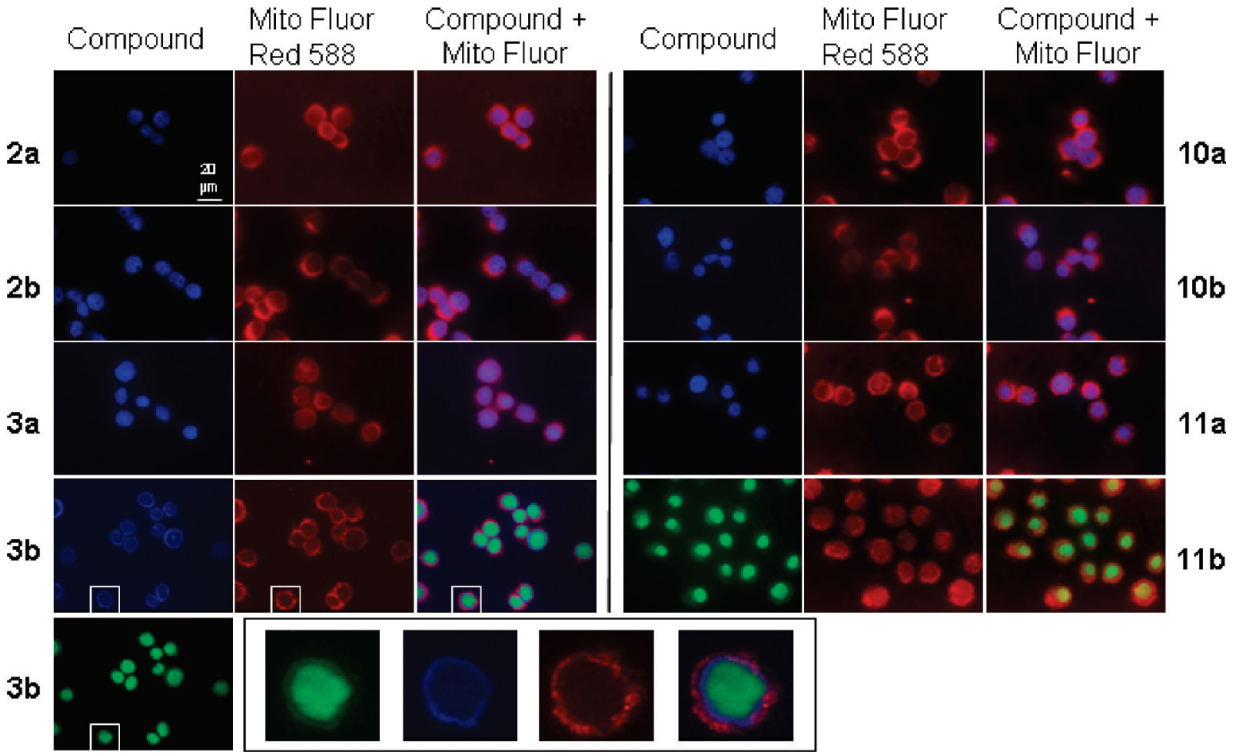

Figure 8. Cell penetration and subcellular localization using fluorescence microscopy. HT-29 human colon carcinoma cells were treated for 16 h with 5 μM of various benzothiazole derivatives specified on each panel side prior to further treatment with Mito Fluor Red 588 used to localize the cytoplasm compartment (middle panels of each series). Single fluorescence analysis of the compounds was established in blue for all compounds with exceptions for compound **11b**, which fluoresces only in green, and compound **3b**, which fluoresces both in blue and in green (left panels of each series). Superposition analyses are presented on the right panels of each series. Enlarged pictures of significant cells from each **3b** panel (as specified using white boxes) are shown in embedded panels at the bottom. The size marker is given in the first panel.

through the cellular and nuclear membranes, we used their fluorescence properties to explore their potential subcellular localization. HT-29 cells were treated with 5 μM of each drug as a fixed concentration of compounds that is sufficient to visualize the compounds using fluorescence microscopy. Mito Fluor Red 588 was used concomitantly as a mitochondrion marker to visualize the cytoplasm. Figure 8 shows the good cellular penetration of this new series and shows the nuclear localization of each tested compound as single fluorescence analyses (left panels of each column) or as superposition with the marker for cytoplasm (right panels of each column). Of particular interest, compound **3b** fluoresces both in green and in blue and reveals a particular localization: when analyzed in green, compound **3b** locates in the nucleus, as determined for other compounds, but when analyzed in blue, it locates at the perinuclear level, as evidenced in the surrounding panels. This particular localization difference might reflect interactions of **3b** with two different types of partners.

Conclusion

In this paper, the synthesis of new amidino- and imidazolinyl-substituted 2,5-dibenzothiazolyl furans and thiophenes (**10a**, **10b**, **11a**, and **11b**) from 2,5-dicarbonylchlorides of furan or thiophene dicarboxylic acids with zwitterionic amidino- or imidazolinyl-substituted aminothiophenoles **8** and **9** has been described. A strong antiproliferative effect of the tested compounds (**2a**, **2b**, **3a**, **3b**, **10a**, **10b**, **11a**, **11b**) was observed on all tested cell lines in a concentration-dependent response pattern. Especially, this was observed on HeLa, MCF-7, and MiaPaCa-2 cell lines where all compounds strongly inhibited the cell growth at submicromolar concentrations and higher. In particular, the strongest antiproliferative effect, in addition to a nonselective cytotoxic activity, was observed for three imidazolinyl-substituted derivatives **3a**, **3b**, and **11b** and for the amidino-substituted thiophene derivative **10b**. The amidino-substituted thiophene derivative **2b** exerted a strong differential antiproliferative effect both on the MCF-7 and MiaPaCa-2 cells, while showing a lower cytotoxicity on normal human fibroblasts in comparison to other highly active compounds. From DNA binding studies, compounds **2a**, **2b**, **3a**, **3b**, **10a**, and 11a were identified as strong DNA binders whereas compounds 10b and **11b** were weaker DNA binding agents (Table 4 and Figures 6 and 7). Using compounds **2a** to **3b**, an isosbestic point is seen for drug concentrations from 0.1 μM up to 4−20 μM depending on the compound, suggesting that a single mode of binding occurs at those concentrations (Supplementary Figure 1A). Using higher DNA concentrations (more than 30 or 40 μM), a second isosbestic point occurs at higher wavelength, suggesting a second mode of binding at those drug/DNA ratios. This is in agreement with observations from DNase I footprinting experiments showing clear sequence selectivity on AT-rich sequences (Figure 7 and Supplementary Figures 3−5) at the lowest concentrations but nonsequence specific binding at highest drug concentration (data not shown). Using DNA concentrations below 20 μM, the CD spectra show a large positive ICD in the presence of both CT-DNA and poly-$(dAdT)_2$ but no ICD using poly$(dGdC)_2$, suggesting a binding within the DNA groove of AT-rich sequences but not that of GC-rich sites. At concentrations greater than 20 μM of the active compounds **2b** and **3b**, an additional negative ICD is observed using both CT-DNA and poly$(dAdT)_2$, whereas a bisignate excitonic ICD is generated using poly$(dGdC)_2$, arguing for a second binding mode (sequence-independent) in correlation with the second isosbestic point evidenced at those concentrations using UV/visible spectrometry (Supplementary Figure 1). Both **10b** and **11b** weak binders bore a thiophene central core instead of the furan within the respective strong binders **10a** and **11a**. The change of the oxygen atom for a sulfur induces an enlargement of the angle of the two amidino or imidazolinyl benzothiazole "arms" of the molecules, which could impair a good fitting of the thiophene-containing molecules on the DNA helix and thus reduce their DNA binding activities, as evidenced using T_m measurements (Table 5) and DNase I footprinting activities (Figure 7 and Supplementary Figures 3−5). Similarly, the same change of the furan core to a thiophene moiety in the imidazolinyl phenyl benzothiazole series (compare **3a** to **3b**) induces changes in sequence specificity: the furan compound **3a** strongly interacted with AT-sites such as the 5′-ATTA sequence, whereas the thiophene compound **3b** failed and showed preference for GC sites as evidenced from T_m measurements on hairpin oligonucleotides. A similar modification does not affect DNA binding affinity and selectivity in the isopropyl amidine series (**2a** versus 2b). This might be due to higher degree of flexibility of those extremities from comparison with amidinyl and imidazolinyl ends to fit with the DNA groove, more likely the minor one. Identification of the binding mode of the different compounds argues for an orientation in the helix axis with the compounds setting in the groove of the DNA helix, as evidenced from CD spectra (Figure 6 and Supplementary Figure 2). Such groove binding occurs on AT-rich sequences, as evidenced from footprinting experiments (Figure 7 and Supplementary Figures 3−5) and CD spectra using poly$(dAdT)_2$ from comparison with poly$(dGdC)_2$ (Supplementary Figure 2). At the highest drug/DNA ratio, interactions of **2b** and **3b** with poly$(dAdT)_2$ result in a positive excitonic effect, suggesting stacking of the molecule in a right-handed orientation parallel to that of DNA helix. Not all AT-containing sequences are equally recognized by those compounds, as evidenced using DNase I footprinting experiments (Figure 7 and Supplementary Figures 3−5) and melting temperature using hairpin oligonucleotides containing specifically designed sequences (Table 5). However, in the presence of pure GC oligonucleotides (poly$(dGdC)_2$), the interaction seems different with negative excitonic cotton effects using compound **2a** whereas (i) compounds **2b** and **3b** present positive exciton chirality, suggesting a right-handed orientation of the molecule similar to that of the DNA helix; (ii) compounds **10a** and **11a** present only negative ICD, suggesting chromophore stacking or intercalation process; and (iii) compound **3a** shows of a mixture of right-handed (in agreement with a fitting in the groove) and chromophore stacking or intercalative orientations.

Compounds **2b** and **3b** were chosen for biological studies due to their differential antiproliferative properties. Both compounds accumulate in the nucleus and act as groove binders, thereby directly inhibiting DNA replication and inducing the S and G2 arrests or the G1 arrest if employing **3b** at higher concentration. Apoptosis induction was observed for both compounds. The biological results presented herein are in line with our previous studies showing that this class of compounds has strong antitumor properties, which might be enhanced in dependence on the position of the substituent on the 2-phenylbenzothiazole skeleton, as well as on the type of amidino substituent attached. Newly designed and efficiently synthesized series of diamidino-, diisopropylamidino-, and diimidazolinyl-substituted derivatives of phenyl benzothiazolyl and dibenzothiazolyl furans and thiophenes described in this study

have shown to be a highly promising class of antitumor compounds. Nevertheless, it was generally observed that the imidazolinyl-substituted derivatives and/or the thiophene core were in correlation with increased antiproliferative activity.

Experimental Section

Chemistry. Melting points were determinate on a Koffler hot stage microscope. IR spectra were recorded on a Nicolet magna 760, with KBr disks or Bruker Vertex 70 FTIR spectrophotometer with an ATR sampling accessory. ^{1}H and ^{13}C NMR spectra were recorded on Bruker Avance DPX 300 or Bruker AV-600 spectrometers using TMS as an internal standard and the deuterated solvents indicated were used. Mass spectra were recorded with an Agilent 1100 Series LC/MSD Trap SL spectrometer using electrospray ionization (ESI). Elemental analyses for carbon, hydrogen, and nitrogen were performed at the microanalytical laboratories of the Rudjer Boskovic Institute. Where analyses are indicated only as symbols of elements, analytical results obtained are within 0.4% of the theoretical value. All compounds were routinely checked by TLC with Merck silica gel 60F-254 glass plates. Synthesis of unsymmetrical bisnitriles **1a** and **1b** and bisamidines **2a**, **2b**, **3a**, and **3b** was achieved as described in Scheme 1 according to the literature.[28,29] Dichlorocarbonyl compounds **5a** and **5b** were prepared from dicarboxylic acid **4a** and **4b** and thionyl chloride prior to use. Compound **7** was prepared from 4-amino-3-sulfanylbenzonitrile **6**[29] and furan-2,5-dicarbonyl dichloride **5a** and reported in Supporting Information. The 5-amidinium-2-aminobenzothiolate **8** and 5-(imidazolinium-2-yl)-2-aminobenzothiolate hydrate **9** described as reagent in Scheme 2 were prepared according to the literature.[30]

General Methods for Preparation of Compounds 10a, 10b, 11a, and 11b. Method A: A mixture of 5-amidinium-2-aminobenzothiolate **8** (0.335 g, 2.0 mmol) or 5-(imidazolinium-2-yl)-2-aminobenzothiolate hydrate **9** (0.423 g, 2.0 mmol) and furan-2,5-dicarboxylic acid **4a** (0.156 g, 1.0 mmol) or thiophene-2,5-dicarboxylic acid **4b** (0.172 g, 1 mmol) in polyphosphoric acid (8−10 g) was heated with stirring for 2 h at 180 °C. The reaction mixture was cooled and poured in water. The resulting precipitate was filtered off, washed with $NaHCO_3$ solution (10%), and dried. The products were crystallized from 10:1 mixture of glacial acetic acid/concentrated hydrochloric acid mixture (charcoal), filtered off, washed with acetone, and dried in vacuum. The pure products were obtained by crystallization from appropriate solvents.

Method B: A mixture of 5-amidinium-2-aminobenzothiolate **8** (0.335 g, 2.0 mmol) or 5-(imidazolinyl-2-yl)-2-aminobenzothiolate hydrate **9** (0.423 g, 2.0 mmol) and furan-2,5-dicarbonyl dichloride **5a** (0.192 g, 1.0 mmol) or thiophene-2,5-dicarbonyl dichloride **5b** (0.208 g, 1.0 mmol) in glacial acetic acid (25 mL) was refluxed for 4 h under nitrogen. The reaction mixture was cooled and the crystals were filtered off, washed with diethylether, and dried. The crystals were suspended in 2 M hydrochloric acid (25 mL), heated to boil, cooled and the resulting hydrochloride salts filtered off, washed with acetone, and dried in vacuum. The pure products were obtained by crystallization from appropriate solvents.

2,2′-(Furan-2,5-diyl)bis(1,3-benzothiazole-6-carboximidamide) dihydrochloride (10a): Compound **10a** was prepared using general Methods A and B described above. Crystallization from a water/acetone mixture afforded 0.296 g (54.3%, Method A) and 0.393 g (72.1%, Method B) of yellow crystals: mp > 300 °C; ^{1}H NMR (300 MHz, DMSO-d_6) (δ ppm) 9.48 (s, 4H, disappeared on addition of D_2O, $4H_{amidine}$), 9.17 (s, 4H, disappeared on addition of D_2O, $4H_{amidine}$), 8.66 (d, 2H, J = 1.4 Hz, $2H_{benzothiazole}$), 8.24 (d, 2H, J = 8.5 Hz, $2H_{benzothiazole}$), 7.90 (dd, 2H, J = 1.6 Hz, J = 8.6 Hz, $2H_{benzothiazole}$), 7.73 (s, 2H, $2H_{furan}$).

2,2′-(Thiophene-2,5-diyl)bis(1,3-benzothiazole-6-carboximidamide) dihydrochloride (10b): Compound **10b** was prepared using general Methods A and B described above. Crystallization from a water/acetone mixture afforded 0.343 g (61.2%, Method A) and 0.495 g (88.2%, Method B) of yellow crystals: mp > 300 °C; ^{1}H NMR (300 MHz, DMSO-d_6) (δ ppm) 9.55 (s, 4H, disappeared on addition of D_2O, $4H_{amidine}$), 9.34 (s, 4H, disappeared on addition of D_2O, $4H_{amidine}$), 8.73 (d, 2H, J = 1.6 Hz, $2H_{benzothiazole}$), 8.25 (d, 2H, J = 8.6 Hz, $2H_{benzothiazole}$), 8.12 (s, 2H, $2H_{thiophene}$), 7.98 (dd, 2H, J = 1.8 Hz, J = 8.6 Hz, $2H_{benzothiazole}$).

2,2′-(Furan-2,5-diyl)bis[6-(4,5-dihydro-1*H*-imidazol-2-yl)-1,3-benzothiazole] dihydrochloride (11a): Compound **11a** was prepared using general Methods A and B described above. Crystallization from a water/acetone mixture afforded 0.181 g (30.3%, Method A) and 0.451 g (75.6%, Method B) of yellow crystals: mp > 300 °C; ^{1}H NMR (300 MHz, DMSO-d_6) (δ ppm) 10.70 (br s, 4H, disappeared on addition of D_2O, $4H_{amidine}$), 8.79 (s, 2H, $2H_{benzothiazole}$), 8.33 (d, 2H, J = 8.6 Hz, $2H_{benzothiazole}$), 7.99 (d, 2H, J = 8.6 Hz, $2H_{benzothiazole}$), 7.80 (s, 2H, $2H_{furan}$), 4.02 (s, 8H, CH_2).

2,2′-(Thiophene-2,5-diyl)bis[6-(4,5-dihydro-1*H*-imidazol-2-yl)-1,3-benzothiazole] dihydrochloride (11b): Compound **11b** was prepared using general Methods A and B described above. Crystallization from a water/acetone mixture afforded 0.218 g (35.6%, Method A) and 0.484 g (78.8%, Method B) of yellow crystals: mp > 300 °C; ^{1}H NMR (300 MHz, DMSO-d_6) (δ ppm) 10.75 (br s, 4H, disappeared on addition of D_2O, $4H_{amidine}$), 8.86 (s, 2H, $2H_{benzothiazole}$), 8.29 (d, 2H, J = 8.6 Hz, $2H_{benzothiazole}$), 8.16 (s, 2H, $2H_{thiophene}$), 8.11 (d, 2H, J = 8.6 Hz, $2H_{benzothiazole}$), 4.05 (s, 8H, CH_2).

Antitumor Activity Assays. The cell lines HeLa (cervical carcinoma), SW620 (colorectal adenocarcinoma, metastatic), MiaPaCa-2 (pancreatic carcinoma), MCF-7 (breast epithelial adenocarcinoma, metastatic), HEp-2 (epidermoid carcinoma, larynx), HepG2 (hepatocellular carcinoma), and JK (normal diploid human fibroblasts) were cultured as monolayers and maintained in Dulbecco's modified Eagle medium (DMEM) supplemented with 10% fetal bovine serum (FBS), 2 mM L-glutamine, 100 U/mL penicillin, and 100 μg/mL streptomycin in a humidified atmosphere with 5% CO_2 at 37 °C.

For the growth inhibition activity assay, the panel cell lines were inoculated onto a series of standard 96-well microtiter plates on day 0, at 3000−5000 cells per well according to the doubling times of specific cell line. Test agents were then added in five 10-fold dilutions (1×10^{-8} to 1×10^{-4} M) and incubated for further 72 h. Working dilutions were freshly prepared on the day of testing in the growth medium. The solvent (DMSO) was also tested for eventual inhibitory activity by adjusting its concentration to be the same as in the working concentrations (DMSO concentration never exceeded 0.1%). After 72 h of incubation, the cell growth rate was evaluated by performing the MTT assay: experimentally determined absorbance values were transformed into a cell percentage growth (PG) using the formulas proposed by National Cancer Institute and described previously in Gazivoda et al.[38] This method directly relies on control cells behaving normally at the day of assay because it compares the growth of treated cells with the growth of untreated cells in control wells on the same plate—the results are therefore a percentile difference from the calculated expected value.

The IC_{50} and LC_{50} values for each compound were calculated from dose−response curves using linear regression analysis by fitting the mean test concentrations that give PG values above and below the reference value. If, however, all of the tested concentrations produce PGs exceeding the respective reference level of effect (e.g., PG value of 50) for a given cell line, the highest tested concentration is assigned as the default value (in the screening data report that default value is preceded by a " > " sign). Each test point was performed in quadruplicate in three individual experiments. The results were statistically analyzed

(ANOVA, Tukey posthoc test at $p < 0.05$). Finally, the effects of the tested substances were evaluated by plotting the mean percentage growth for each cell type in comparison to control on dose−response graphs.

Cell Cycle Analysis. A total of 5×10^5 cells were seeded per Petri dish (10 cm in diameter, Sarstedt, Germany). After 24 h, MCF-7 cells were treated with the compound **2b** at concentrations of 10 and 50 μM, and MiaPaCa-2 and MCF-7 cells were treated with compound **3b** at concentrations of 1 and 5 μM. After 24 and 48 h, the attached cells were trypsinized, combined with floating cells, washed with PBS, and fixed with 70% ethanol. Immediately before the analysis, the cells were washed again with PBS and stained with 1 μg/mL of propidium iodide (PI) with the addition of 0.2 μg/mL of RNase A. The stained cells were then analyzed with Becton Dickinson FACScalibur flow cytometer (10 000 counts were measured). Each test point was performed in duplicate. The percentage of the cells in each cell cycle phase was based on the obtained DNA histograms and determined using the WinMDI 2.9 and Cylchred software. Statistical analysis was performed in Microsoft Excel by using the ANOVA at $p < 0.05$.

Detection of Apoptosis, Annexin V Assay. Detection and quantification of apoptotic cells at a single cell level was performed using Annexin V-Fluos staining kit (Roche), according to the manufacturer's recommendations. The MCF-7 cells were seeded in chamber slides (4×10^4 cells/well, Lab-Tk II Chamber slide, Nunc, SAD) and treated with compounds **2b** (concentrations 10 and 50 μM) and compound **3b** (1 and 5 μM). The MiaPaCa-2 cells were also seeded in 6-well plates (4×10^4 cells/well, Lab-Tk II Chamber slide, Nunc, SAD) and treated only with compound **3b** (1 and 5 μM). After 24 and 48 h, the growth medium was removed from wells and 100 μL of incubation buffer, containing Annexin V-Flous labeling reagent and propidium iodide (PI) solution, was added per well and incubated for 15 min. The cells were then washed with PBS with the addition of 2% FCS, pelleted, and resuspended in two staining solutions prepared in the Hepes buffer containing either Annexin V-fluorescein labeling reagent, propidium iodide (PI), or their combination. Camptothecin (20 μM, Sigma) was used as the control apoptosis-inducing agent. The cells were then analyzed under the fluorescent microscope. The results are represented as percentages of cells positive to annexin and/or propidium iodide per total cell number. At least 100 cells were counted in each well.

UV/Visible Absorption Spectroscopy and DNA Melting Temperature Studies. CT-DNA, double-stranded poly(dAdT)$_2$, and poly(dGdC)$_2$ oligonucleotides were purchased from Sigma. CT-DNA was prepared as previously described (David-Cordonnier et al.). Compounds **2a**, **3a**, **3b**, **10b**, **11a**, and **11b** were dissolved at 10 mM in DMSO, whereas compounds **2b** and **10a** were prepared as 5 and 4 mM solutions, respectively. Each compound was further extemporarily diluted in the appropriate aqueous reaction buffers.

UV/visible spectral absorption measurements were conducted using a fixed concentration (20 μM) of the various tested drugs incubated in 1 mL of BPE buffer (6 mM Na_2HPO_4, 2 mM NaH_2PO_4, 1 mM EDTA, pH 7.1) in the presence or absence of graded concentrations of CT-DNA (from 0.1 to 200 μM of base pairs) in a quartz cuvette of 10 mm path length. The UV/visible spectra were recorded from 300 to 450 nm using a Uvikon 943 spectrophotometer and are referenced against a cuvette containing the same graded concentrations of CT-DNA as that in the cuvette sample to directly substrate intrinsic CT-DNA absorption. The binding constant, K, was determined from the spectroscopic titration data using the following equation $[\text{CT-DNA}]/(\varepsilon_{\text{Free}} - \varepsilon_{\text{Obs}}) = [\text{CT-DNA}]/(\varepsilon_{\text{Bound}} - \varepsilon_{\text{Free}}) + 1/K(\varepsilon_{\text{Bound}} - \varepsilon_{\text{Free}})$, where ε_{Obs}, $\varepsilon_{\text{Free}}$, and $\varepsilon_{\text{Bound}}$ correspond to A /[compound], the extinction coefficient for the free compound, and the extinction coefficient for the compound fully bound to CT-DNA, respectively. By plotting $[\text{CT-DNA}]/(\varepsilon_{\text{Free}} - \varepsilon_{\text{Obs}})$ versus [CT-DNA] (Supplementary Figure 1B), K is given by the ratio of the slope to the intercept.

The variations of melting temperature (ΔT_m) of CT-DNA or poly(dAdT)$_2$ induced by the presence of the various compounds were calculated from the melting temperature measurement of 20 μM CT-DNA or poly(dAdT)$_2$ incubated alone (control T_m) or with 2 μM of the various compounds (drug/base pair ratio of 0.1) in 1 mL of BPE buffer. The ΔT_m induced by the various compounds on specific sites was measured at a drug/number of site ratio of 0.1 using 2 μM of 22-mer hairpin oligonucleotides (the 9 bp stem generated from autohybridization is underlined) designed to specifically contain one site of interest (in bold): ATTA (5′-CGC**ATTA**CGTCTCCG**TAAT**GCG-3′); AATT (5′-CGC**AATT**CGTCTCCG**AATT**GCG-3′); TTAA (5′-CGC-**TTAA**CGTCTCCG**TTAA**GCG-3′); GCGC (5′-AGT**GCGC**-TGTCTCCA**GCGC**ACT-3′) and ACCA (5′-CGC**ACCA**CGT-CTCCG**TGGT**GCG-3′) in the absence or presence of 2 μM of the specified compounds. The absorbency of DNA at 260 nm was measured in quartz cells using the Uvikon 943 spectrophotometer thermostatted with a Neslab RTE111 cryostat. Absorption value was measured for each sample every minute over a range of 20 to 100 °C with an increment of 1 °C per min. The T_m values were obtained from the midpoint of the hyperchromic transition, and the variation of melting temperature was calculated from the equation ΔT_m values = $T_{m[\text{Drug+DNA}]} - T_{m[\text{DNA alone}]}$.

Fluorescence Spectroscopy. Fluorescence spectral measurement were recorded using 1 or 5 μM of the fluorescent drugs (as specified in the figure legend) incubated in 1 mL of BPE buffer in the presence or absence of increasing concentrations of CT-DNA (0.1 to 30 μM of base pairs or below if precipitation of the CT-DNA was observed in the sample) in a quartz cuvette of 10 mm path length. The excitation wavelengths were 380 (compounds **2a** and **2b**), 386 (compounds **3a**, **3b** and **10a**), 318 (compound **11a**), 388 (compound **10b**), and 392 nm (compound **11b**). The quenching constant K_{SV} was deduced from Stern−Volmer plots expressing the ratio of fluorescence of the compound alone (F_0) over the fluorescence of the compound in the presence of CT-DNA (F) as a function of CT-DNA concentration. In this configuration, $F_0/F = 1 + K_{SV}[\text{CT-DNA}]$, where the slope K_{SV} is considered as an equilibrium constant for the static quenching process.

Circular Dichroism. A fixed concentration of CT-DNA (200 μM of base pairs) was incubated with or without (control) increasing concentrations of the different drugs (from 1 to 25 μM for compounds **2a**, **2b**, and **3a** or from 1 to 50 μM for the other compounds) in 1 mL of sodium cacodylate (1 mM, pH 7.0). The analyses using poly(dAdT)$_2$ or poly-(dGdC)$_2$ (200 μM of base pairs) were performed using incremented drug concentration from 2 to 80 μM. The CD spectra were collected from 530 to 230 nm with a resolution of 0.1 nm, in a quartz cell of 10 mm path length, using a J-810 Jasco spectropolarimeter at 20 °C controlled by a PTC-424S/L peltier type cell changer (Jasco).

DNase I Footprinting. DNase I footprinting experiments were performed essentially as described in Peixoto et al.[39] Briefly, the 265 and 117 bp DNA fragments were obtained from double digestion of the pBS plasmid (Stratagene, La Jolla, CA) at *Eco*RI and *Pvu*II restriction sites for 1 h with the corresponding enzymes in their respective buffers. Similarly, the 257 bp DNA fragment was generated from *Bam*HI and *Pci*I digestion of pGL3cat-basic vector (Promega). The generated DNA fragments were 3′-end labeled using 5 μL of α-[^{32}P]-dATP (265 and 117 bp fragments) or α-[^{32}P]-dGTP (3000 Ci/mmol each, GE Healthcare, Buckinghamshire, England) and 10 units of Klenow enzyme (BioLabs) for 30 min at 37 °C. The resulting radiolabeled DNA fragments were then separated from the plasmid remnant on a 6% polyacrylamide gel under native conditions in TBE buffer (89 mM Tris base, 89 mM boric acid, 2.5 mM Na_2 EDTA, pH 8.3). The portion of the gel containing the DNA fragments was cut off from the gel, crushed, and dialyzed overnight against 400 μL of elution buffer (10 mM Tris-HCl pH 8.0, 1 mM EDTA, 100 mM NaCl). The DNA was recovered

from polyacrylamide gel by filtration through a Millipore 0.22 μm membrane and subsequently precipitated with cold ethanol followed by centrifugation. Appropriate concentrations of the various ligands (as indicated in the figures legend) were incubated with the radio-labeled DNA fragments for a 15 min incubation at 37 °C to ensure equilibrium prior to digestion of the DNA by the addition of DNase I (final concentration 0.001 unit/mL) in 20 mM NaCl, 2 mM $MgCl_2$, 2 mM $MnCl_2$, pH 7.3. After 3 min of digestion, the reaction was stopped by freeze-drying. Samples were lyophilized and subsequently dissolved in 4 μL of denaturing loading buffer (80% formamide solution containing tracking dyes). The DNA samples were heated at 90 °C for 4 min and rapidly chilled on ice for 4 min prior to electrophoresis. The generated DNA cleavage products were resolved on a denaturing polyacrylamide gel (0.35 mm thick, 8% polyacrylamide containing 8 M urea). After a 90 min electrophoresis at 65 W in TBE buffer, gels were soaked in 10% acetic acid for 10 min, transferred to Whatman 3 MM paper, and dried under vacuum at 80 °C. A Molecular Dynamics STORM 860 was used to collect data from storage screens exposed to dried gels overnight at room temperature. The identity of the bases was established from comparison of the relative position of the bands to the guanines sequencing standard (G-track) classically obtained using dimethylsulfate and piperidine treatment of the same DNA fragment. Quantifications of the footprint were performed using ImageQuant 3.3 software.

Fluorescence Microscopy. HT-29 human colon carcinoma cells (ATCC) were maintained as monolayers in 150 cm^2 culture flasks using culture medium consisting of DMEM-glutaMAX medium supplemented with 10% fetal bovine serum, penicillin (100 IU/mL), and streptomycin (100 μg/mL); 5×10^4 HT-29 cells were cultured in Lab-Tek II Chamber Slide (Nunc Int.) incubated with 5 μM of the tested compounds for 16 h at 37 °C in culture medium. Cells were then rinsed three times with ice-cold PBS prior to be incubated in the dark with 250 nM of the fluorescent cytoplasmic probe Mito Fluor Red 588 (Molecular Probes) for 30 min at 37 °C. After a further three washings with PBS, a drop of Vectashield antifade solution (AbCys S.A., France) was then added and the treated portion of the slide was visualized immediately by fluorescence microscopy using an ApoTome microscope (Zeiss) with an X63 oil-immersion objective. Images were captured using the software AxioVision with an excitation wavelength of 358 nm for an emission at 461 nm in blue for all compounds but **11b**, for which the excitation wavelength was 495 nm for an emission at 519 nm (green). Compound **3b** was analyzed at both blue and green fluorescence. The used excitation and emission wavelengths for Mito Fluor Red 588 were 588 and 622 nm, respectively.

Acknowledgment. We greatly appreciate the financial help of the Croatian Ministry of Science Education and Sports (Projects 125-0982464-1356, 098-0982464-2393, 117-0000000-3283). M.-H.D.-C. thanks the Fonds européen de développement régional (FEDER, European Community) and the Région Nord-Pas de Calais for a grant and a fellowship to S.D., the Ligue Nationale contre le Cancer (Comité du Nord) and the Institut pour la Recherche sur le Cancer de Lille (IRCL) for grants. R.N. is supported by the CHRU de Lille and the Conseil Régional Nord-Pas de Calais for her Ph.D. fellowship. We are grateful to the IRCL for a postdoctoral fellowship to P.P. and technical expertise (M.-P.H.). The Institut de Médecine Prédictive et de Recherche Thérapeutique (IMPRT)−IFR114 is acknowledged for access to the Molecular Dynamics STORM 860 equipment.

Supporting Information Available: Experimental and spectroscopic data for cyano derivative **7**, elemental analysis and spectroscopic data for new compounds (**10a**, **10b**, **11a**, **11b**) as well as the UV/visible absorbance spectrometry data, the DNase I footprinting assay on the 257 bp DNA fragment and the densitometric analyses of DNase I footprinting assays on the 257 and 117 bp DNA fragments. This material is available free of charge via the Internet at http://pubs.acs.org.

References

(1) Ban, M.; Taguchi, H.; Katsushima, T.; Takahashi, M.; Shinoda, K.; Watanabe, A.; Tominaga, T. Novel antiallergic and antiinflammatory agents. Part I: Synthesis and pharmacology of glycolic amide derivatives. *Bioorg. Med. Chem.* **1998**, *6*, 1069–1076.

(2) Papadopoulou, C.; Geronikaki, A.; Hadjipavlou-Litina, D. Synthesis and biological evaluation of new thiazolyl/benzothiazolyl-amides, derivatives of 4-phenyl-piperazine. *Farmaco* **2005**, *60*, 969–973.

(3) Chung, Y.; Shin, Y.-K.; Zhan, C.-G.; Lee, S.; Cho, H. Synthesis and evaluation of antitumor activity of 2- and 6-[(1,3-benzothiazol-2-yl)aminomethyl]-5,8-dimethoxy-1,4-naphthoquinone derivatives. *Arch. Pharm. Res.* **2004**, *27*, 893–900.

(4) McFadyen, M. C. E.; Melvin, W. T.; Murray, G. I. Cytochrome *P*450 enzymes: novel options for cancer therapeutics. *Mol. Cancer Ther.* **2004**, *3*, 363–371.

(5) Yoshida, M.; Hayakawa, I.; Hayashi, N.; Agatsuma, T.; Oda, Y.; Tanzawa, F.; Iwasaki, S.; Koyama, K.; Furukawa, H.; Kurakata, S. Synthesis and biological evaluation of benzothiazole derivatives as potent antitumor agents. *Bioorg. Med. Chem. Lett.* **2005**, *15*, 3328–3332.

(6) Starčević, K.; Ćaleta, I.; Cinčić, D.; Kaitner, B.; Kralj, M.; Ester, K.; Karminski-Zamola, G. Synthesis, crystal structure determination and antiproliferative evaluation of novel benzazoyl benzamides. *Heterocycles* **2006**, *68*, 2285–2299.

(7) Ćaleta, I.; Kralj, M.; Bertoša, B.; Tomić, S.; Pavlović, G.; Pavelić, K.; Karminski-Zamola, G. Novel cyano and amidinobenzothiazole derivatives: synthesis, antitumor evaluationand X-ray quantitative structure-activity relationship (QSAR) analysis. *J. Med. Chem.* **2009**, *52*, 1744–1756.

(8) Baell, J. B.; Forsyth, S. A.; Gable, R. W.; Norton, R. S.; Mulder, R. J. Design and synthesis of type-III mimetics of ω-conotoxin GVIA. *J. Comput.-Aided Mol. Des.* **2002**, *15*, 1119–1136.

(9) Westway, S. M.; Thompson, M.; Rami, H. K.; Stemp, G.; Trouw, L. S.; Mitchell, D. J.; Seal, J. T.; Medhurst, S. J.; Lappin, S. C.; Biggs, J.; Wright, J.; Arpino, S.; Jerman, J. C.; Cryan, J. E.; Holland, V.; Winborn, K. Y.; Coleman, T.; Stevens, A. J.; Davis, J. B.; Gunthorpe, M. J. Design and synthesis of 6-phenylnicotinamide derivatives as antagonists of TRPV1. *Bioorg. Med. Chem. Lett.* **2008**, *18*, 5609–5613.

(10) Das, J.; Lin, J.; Moquin, R. V.; Shen, Z.; Spergel, S. H.; Wityak, J.; Doweyko, A. M.; DeFex, H. F.; Fang, Q.; Pang, S.; Pitt, S.; Ren Shen, D.; Schieven, G. L.; Barrish, J. C. Molecular design, synthesis, and structure−activity relationships leading to the potent and selective $P56^{lck}$ inhibitor BMS-243117. *Bioorg. Med. Chem. Lett.* **2003**, *13*, 2145–2149.

(11) Das, J.; Moquin, R. V.; Lin, J.; Liu, C.; Doweyko, A. M.; DeFex, H. F.; Fang, Q.; Pang, S.; Pitt, S.; Ren Shen, D.; Schieven, G. L.; Barrish, J. C.; Wityak, J. Discovery of 2-amino-heteroaryl-benzothiazole-6-anilides as potent $p56^{lck}$ inhibitors. *Bioorg. Med. Chem. Lett.* **2003**, *13*, 2587–2590.

(12) Gaillard, P.; Jeanclaude-Etter, I.; Ardissone, V.; Arkinstall, S.; Cambet, Y.; Camps, M.; Chabert, C.; Church, D.; Cirillo, R.; Gretener, D.; Halazy, S.; Nichols, A.; Szyndralewiez, C.; Vitte, P.-A.; Gotteland, J.-P. Design and synthesis of the first generation of novel potent, selective, and in vivo active (benzothiazol-2-yl)acetonitrile inhibitors of the c-Jun N-terminal kinase. *J. Med. Chem.* **2005**, *48*, 4596–4607.

(13) Liu, C.; Lin, J.; Pitt, S.; Zhang, R. F.; Sack, J. S.; Kiefer, S. E.; Kish, K.; Doweyko, A. M.; Zhang, H.; Marathe, P. H.; Trzaskos, J.; Mckinnon, M.; Dodd, J. H.; Barrish, J. C.; Schieven, G. L.; Leftheris, K. Benzothiazole based inhibitors of p38a MAP kinase. *Bioorg. Med. Chem. Lett.* **2008**, *18*, 1874–1879.

(14) Pinar, A.; Yurdakul, P.; Yildiz, I.; Temiz-Arpaci, O.; Acan, N. L.; Aki-Sener, E.; Yalcin, I. Some fused heterocyclic compounds as eukaryotic topoisomerase II inhibitors. *Biochem. Biophys. Res. Commun.* **2004**, *317*, 670–674.

(15) Abdel-Aziz, M.; Matsuda, K.; Otsuka, M.; Uyeda, M.; Okawara, T.; Suzuki, K. Inhibitory activities against topoisomerase I & II by polyhydroxybenzoyl amide derivarives and their structure−activity relationship. *Bioorg. Med. Chem. Lett.* **2004**, *14*, 1669–1672.

(16) Manjula, S. N.; Malleshappa, N.; Noolvi, K.; Vipan Parihar, S. A.; Reddy, M.; Ramani, V.; Gadad, A. K.; Singh, G. N.; Gopalan Kutty, C.; Rao, M. Synthesis and antitumor activity of optically

active thiourea and their 2-aminobenzothiazole derivatives: a novel class of anticancer agents. *Eur. J. Med. Chem.* **2009**, *44*, 2923–2929.
(17) Repicky, A.; Jantova, S.; Cipak, L. Apoptosis induced by 2-acetyl-3-(6-methoxybenzothiazo)-2-yl-amino-acrylonitrile in human leukemia cells involves ROS-mitochondrial mediated death signaling and activation of p38 MAPK. *Cancer Lett.* **2009**, *277*, 55–63.
(18) Tasler, S.; Müller, O.; Wieber, T.; Herz, T.; Krauss, R.; Totzke, F.; Kubbutat, M. H. G.; Schächtele, C. N-Substituted 2′-(aminoaryl)-benzothiazoles as kinase inhibitors: hit identification and scaffold hopping. *Bioorg. Med. Chem. Lett.* **2009**, *19*, 1349–1356.
(19) Chaires, J. B.; Ren, J.; Hamelberg, D.; Kumar, A.; Pandya, V.; Boykin, D. W.; Wilson, W. D. Structural selectivity of aromatic diamidines. *J. Med. Chem.* **2004**, *47*, 5729–5742.
(20) Cai, X.; Gray, P. J, Jr.; Von Hoff, D. D. DNA minor groove binders: back in the groove. *Cancer Treat. Rev.* **2009**, *35*, 437–450.
(21) Lansiaux, A.; Dassonneville, L.; Facompré, M.; Kumar, A.; Stephens, C. E.; Bajic, M.; Tanious, F.; Wilson, W. D.; Boykin, D. W.; Bailly, C. Distribution of furamidine analogues in tumor cells: influence of the number of positive charges. *J. Med. Chem.* **2002**, *45*, 1994–2002.
(22) Lansiaux, A.; Tanious, F; Mishal, Z.; Dassonneville, L.; Kumar, A.; Stephens, C. E.; Hu, Q.; Wilson, W. D.; Boykin, D. W.; Bailly, C. Distribution of furamidine analogues in tumor cells: targeting of the nucleus or mitochondria depending on the amidine substitution. *Cancer Res.* **2002**, *62*, 7219–7229.
(23) Munde, M.; Ismail, M. A.; Arafa, R.; Peixoto, P.; Collar, C. J.; Liu, Y.; Hu, L.; David-Cordonnier, M.-H.; Lansiaux, A.; Bailly, C.; Boykin, D. W.; Wilson, W. D. Design of DNA minor groove binding diamidines that recognize GC base pair sequences: a novel dimeric-hinge motif. *J. Am. Chem. Soc.* **2007**, *129*, 13732–13743.
(24) Miao, Y.; Lee, M. P.; Parkinson, G. N.; Batista-Parra, A.; Ismail, M. A.; Neidle, S.; Boykin, D. W.; Wilson, W. D. Out-of-shape DNA minor groove binders: induced fit interactions of heterocyclic dications with the DNA minor groove. *Biochemistry* **2005**, *44*, 14701–14708.
(25) Tanious, F. A.; Laine, W.; Peixoto, P.; Bailly, C.; Goodwin, K. D.; Lewis, M. A.; Long, E. C.; Georgiadis, M. M.; Tidwell, R. R.; Wilson, W. D. Unusually strong binding to the DNA minor groove by a highly twisted benzimidazole diphenylether: induced fit and bound water. *Biochemistry* **2007**, *46*, 6944–6956.
(26) Racanè, L.; Tralić-Kulenović, V.; Kitson, R. P.; Karminski-Zamola, G. Synthesis and antiproliferative activity of cyano and amidino substituted 2-phenylbenzothiazoles. *Monatsh. Chem.* **2006**, *137*, 1571–1577.
(27) Racanè, L.; Stojković, R.; Tralić-Kulenović, V.; Karminski-Zamola, G. Synthesis and antitumor evaluation of novel derivatives of 6-amino-2-phenylbenzothiazoles. *Molecules* **2006**, *11*, 325–333.
(28) Racanè, L.; Tralić-Kulenović, V.; Fišer-Jakić, L.; Boykin, W. D.; Karminski-Zamola, G. Synthesis of bis-substituted amidinobenzothiazoles as potential anti-HIV agents. *Heterocycles* **2001**, *55*, 2085–2098.
(29) Tralić-Kulenović, V; Karminski-Zamola, G.; Racanè, L.; Fišer-Jakić, L. Synthesis of symmetric and unsymetric bis cyanosubstituted heterocycles. *Heterocycl. Commun.* **1998**, *4*, 423–427.
(30) Racanè, L.; Tralić-Kulenović, V.; Mihalić, Z.; Pavlović, G.; Karminski-Zamola, G. Synthesis of new amidino-substituted 2-aminothiophenole: mild basic ring opening of benzothiazole. *Tetrahedron* **2008**, *64*, 11594–11602.
(31) Pinar, A.; Yurdakul, P.; Yildiz, I; Temi-Arpaci, O.; Acan, N. L.; Aki-Sener, E; Yalcin, I. Some fused heterocyclic compounds as eukaryotic topoisomerase II inhibitors. *Biochem. Biophys. Res. Commun.* **2004**, *317*, 670–674.
(32) Abdel-Aziz, M.; Matsuda, K.; Otsuka, M.; Uyeda, M.; Okawara, T.; Suzuki, K. Inhibitory activities against topoisomerase I & II by ployhydroxybenzoyl amide derivatives and their structure−activity relationship. *Bioorg. Med. Chem. Lett.* **2004**, *14*, 1669–1672.
(33) Okada, H.; Mak, T. W. Pathways of apoptotic and non-apoptotic death in tumour cells. *Nat. Rev. Cancer* **2004**, *4*, 592–603.
(34) Díaz, L. F.; Chiong, M.; Quest, A. F. G.; Lavandero, S.; Stutzin, A. Mechanisms of cell death: molecular insights and therapeutic perspectives. *Cell Death Differ.* **2005**, *12*, 1449–1456.
(35) Zhang, J.; Cheng, C.; He, C.-L.; Zhou, Y.-J.; Cao, Y. The expression of Bcl-XL, Bcl- XS and p27Kip1 in topotecan-induced apoptosis in hepatoblastoma HepG2 cell line. *Cancer Invest.* **2008**, *26*, 456–463.
(36) Joe, A. K.; Liu, H.; Suzui, M.; Vural, M. E.; Xiao, D.; Weinstein, I. B. Resveratrol induces growth inhibition, S-phase arrest, apoptosis, and changes in biomarker expression in several human cancer cell lines. *Clin. Cancer Res.* **2002**, *8*, 893–903.
(37) Peixoto, P.; Bailly, C.; David-Cordonnier, M.-H. In *Methods in Molecular Biology Series, Drug−DNA Interactions*; Fox, K. R., Ed.; Humana Press: Totowa, NJ, 2010; Vol. 613, pp 235−256.
(38) Gazivoda, T.; Raić-Malić, S.; Krištafor, V.; Makuc, D.; Plavec, J.; Bratulic, S.; Kraljević Pavelić, S.; Pavelić, K.; Naesens, L.; Andrei, G.; Snoeck, R.; Balzarini, J.; Mintas, M. The novel pyrimidine and purine derivatives of l-ascorbic acid: synthesis, one- and two-dimensional ^{1}H and ^{13}C NMR study, cytostatic and antiviral evaluation. *Bioorg. Med. Chem.* **2008**, *16*, 5624–5634.
(39) Peixoto, P.; Liu, Y.; Depauw, S.; Hildebrand, M.-P.; Boykin, D. W.; Bailly, C.; Wilson, W. D.; David-Cordonnier, M.-H. Direct inhibition of the DNA-binding activity of POU transcription factors Pit-1 and Brn-3 by selective binding of a phenyl-furan-benzimidazole dication. *Nucleic Acids Res.* **2008**, *36*, 3341–3353.